THE DEVELOPMENT OF AN ELECTRICALLY HEATED SHOCK DRIVEN TEST FACILITY

by

W. R. Warren
D. A. Rogers
C. J. Harris

Second Symposium on Hypervelocity Techniques

Sponsored by the University of Denver

20-21 March 1962

Denver, Colorado

General Electric Company
Space Sciences Laboratory
Missile and Space Vehicle Department
King of Prussia, Pennsylvania

INTRODUCTION

The shock tube has been used for many years for the generation of gas flows of high energy and high purity (1) (2)[1]. The most general early use of the high temperature shock tube was the extension of the basic knowledge of the properties of many gases; however, with the development of re-entry vehicles, the shock tube was also adapted to the study of many high temperature aerodynamic problems. For example, hypersonic heat transfer problems associated with bodies re-entering the earth's atmosphere at velocities to approximately the satellite value (26,000 ft/sec) were investigated. References 3 and 4 are examples of this type of shock tube application. Because of its ability to produce high temperature gases at relatively high pressure levels, the shock tube was also attractive for the powering of wind tunnels. These tools, generally referred to as shock tunnels, are discussed in references 5 to 8.

The shock tube and shock tunnel have, as a prime characteristic, the ability to produce wide ranges of gas property values. However, most facilities now in existence have restricted performance when simulation of flight conditions at very high velocities is desired. With the current interest in velocities greater than the orbital velocity -- space vehicles will return to earth at velocities equal to and greater than the escape velocity (approximately 36,000 ft/sec) -- it is important to look to methods for extending the ranges of operation of these shock driven tools.

The limits on present facilities are caused to a large extent by the limits that exist on driver gas properties. This is illustrated in Fig. 1 in which is shown the theoretical shock Mach number performance for a simple air shock tube with several types of drivers. For the production of high M_s values, it is important that the driver gas have a high speed of sound. This suggests both that the molecular weight of the gas be low and that its temperature be high. The advantage of these properties in terms of producing strong shocks is seen in Fig. 1. Only two of the many currently used driver techniques are considered: room temperature hydrogen and the products of combustion of a mixture of hydrogen and oxygen (stoichiometric) diluted by helium. Also shown is a band of operating conditions that would be available with high temperature helium drivers. It can be seen that the performance advantage of heated helium over the more conventional drivers is appreciable, particularly since the stagnation enthalpy of the driven gas is closely proportional to M_s^2. Thus, if a helium driver in the range of T_4 levels shown could be produced, the shock velocity performance of shock tubes could be increased considerably.

A question that may now be asked is: what would this increase in M_s capability mean in terms of experimental utility? In attempting to answer this, two facility configurations -- a straight shock tube and a reflected shock tunnel -- will be analyzed briefly. Theoretical shock tube calculations throughout the paper assume that air is in thermodynamic and chemical equilibrium -- using the data of Ziemer (9) -- and that helium is an ideal gas. Fig. 2 shows the performance of a particular shock tube design in terms of simulated flight velocity and altitude. These results are for a driver pressure of 1,000 atmospheres, which appears to

---

[1] Numbers in ( ) refer to references listed at end of paper.

be a practical value. It can be seen that if it is desired to study, for example, shock wave structure in the 35,000 to 40,000 ft/sec regime at altitudes of interest in re-entry (below 300,000 ft), we must look to the development of driver techniques with capabilities similar to those of the heated helium curves in Fig. 2. In Fig. 3, critical performance parameters for a reflected shock tunnel are shown. The T_4 value required for production of a tailored interface wave pattern (10) (11) is shown as a function of M_s.[1] Also given are the simulated flight velocities based on h_5 It can be seen that if a helium driver in the 4000° to 8000° K T_4 range could be produced, tailored conditions would be possible in the 28,000 to 41,000 ft/sec u_f range. Tailored operation with the combustion and hydrogen drivers is significantly below this range. Important problems of the reflected shock tunnel involve, first, the state of the gas during expansion through the nozzle and, second, the degree of simulation of flight conditions at the test section. Several recent studies (12) (13) (14) have shown that appreciable non-equilibrium effects can exist during expansion and that these are reduced by going to higher pressures in region 5. Shown in Fig. 3 are the P_5 levels possible with the heated helium driver technique. These are relatively high but it is probable that some non-equilibrium effects will still exist in the test section unless we go to P_4 levels of several thousand atmospheres. While it is not yet clear that such operation will provide useful flight simulation at high enthalpies, it does appear worthwhile to work toward this end as a possible goal. Even if the flight simulation application proves not to be feasible, the tailored shock tunnel would still provide a useful tool for the study both of expansion processes and of properties of high temperature gases in the reflected region.

On the basis of the above brief discussions, the desirability of a high temperature, low molecular weight driver, such as that presented by the heated helium performances given in Figs. 1 to 3, for use in shock tube and tunnel applications appears to be well established. Consideration must now be given to how it can be produced. Axial uniformity in the heated driver is a strong requirement since it is desired to conduct experiments in relatively uniform steady flows (although these flows will be only several microseconds in duration in some cases). Thus, electromagnetic drivers of the type described in references 15 and 16 would not be appropriate although they produce very strong incident waves. Methods involving heating the driver gas externally and passing it rapidly into the driven tube at high pressure are not satisfactory for the high temperatures under consideration because of the necessity of containing the heated gas in relatively cold wall reservoirs for extended periods of time.

One way to produce a high, uniformly distributed gas temperature in a tubular driver is through the electrical discharge along the axis of the driver of energy stored in capacitors. This was the approach taken during the present study. If the energy exchange can be accomplished fairly efficiently and in a short period of time compared to the characteristic time required for energy to be absorbed by the cool retaining walls, a high temperature driver can be pro-

---

[1] For purposes of discussion, it will be assumed that tailored interface operation is required for the reflected shock tunnel. The use of the equilibrium interface concept (5) can extend long time operation of the shock tunnel to somewhat higher M_s values than that associated with exact tailoring (19).

duced. An inherent advantage of rapidly discharging the energy is that the current path is kept largely within the gas; that is, current is not passed along the wall surface where it would be rapidly dissipated to the wall materials. This leads to high electrical energy conversion efficiency. The diaphragm is also an important part of the system: it must remain intact during the energy discharge process; it must then rupture cleanly and very rapidly.

The purpose of this paper is to describe the progress that has been made in the development and evaluation of an electrically heated helium shock driven facility. The work covered is concerned primarily with a small prototype shock tube. While this tube does not completely meet the requirements one would establish for an ultimate test facility, results from its study do indicate that the attractive features of high performance shock tubes discussed earlier can be achieved. One interesting result of this work is that the prototype facility itself has been found to be useful in the study of hypervelocity stagnation region convective heat transfer problems.

MECHANICAL AND ELECTRICAL DESIGN

The two major requirements which had to be met in developing an electrically heated high enthalpy driver were: that the energy be added uniformly along the length of the driver; and, that the energy be added rapidly enough to prevent excessive heat loss to the walls before diaphragm rupture. The use of an exploding wire along the driver axis to create a path for the arc column was selected as being the simplest approach to meeting the uniform heating requirement. An axial discharge in a coaxial driver circuit also possesses the advantages of low inductance and relatively high resistance, thus helping to assure a minimum discharge time. A capacitive energy storage circuit is used because of its relatively low cost and its capability for short discharge time.

The driver dimensions were selected to provide a practical test of techniques. The design of the tube is shown in Fig. 4. The driver shell is Type 304 stainless steel having a 2 1/4" inside diameter, 18" inside length, and 2" thick walls. Lexan is used for electrical insulation of the driver wall and high voltage electrode. It provides high impact strength, dimensional stability, and thermal shock resistance. The inside wall of the driver is a cylindrical Lexan sleeve with 1/4" wall thickness and is sealed at the electrode end by a Lexan end cap and polyethylene washer. The helium inlet is near the center of the steel shell and enters the driver at the diaphragm end (via a slot in the Lexan sleeve), in order to assure continuity of the insulation.

The high voltage electrode is a hollow copper cylinder 3/8" in diameter which threads into a Lexan insulator. A 1/8" diameter brass rod is inserted through the center of the main electrode and insulated from it by Teflon tubing which also provides a pressure seal in conjunction with a tapered steel washer and nut. The tungsten exploding wire (commonly 5 mil) is attached to a steel

spider at the diaphragm end of the driver and, by about a one inch piece of cotton thread, to the copper main electrode. Adjustment of the amount that the brass electrode extends beyond the main electrode sets the breakdown voltage. This adjustment is made with the main capacitor bank disconnected using a small capacitor to prevent breaking the wire. This technique for initiating the discharge has been very effective as a switching method and permits wide variation of the energy input ($1/2\ CV^2$) with precise control.

The electrical circuit for the driver system is shown schematically in Fig. 5A. Energy storage is provided by forty-seven capacitors, each rated at five microfarads and 20,000 volts. Paralleling is accomplished by two pair of low inductance bus bars running the length of the cart and jumpered at the front end of the capacitor cart. A short bus bar section, which may be removed to facilitate replacing the exploding wire and setting the spark gap, provides capacitor connection to the driver. The equivalent capacitor and bus bar inductance, L_1, is approximately 0.15 microhenry. The driver inductance, L_2, and resistance, R_1, are not calculable during the discharge, but depend on the conditions of the heated plasma. They can be inferred from measurement of the discharge current. A coaxial shunt whose resistance, R_2, is 0.62 miliohm and whose inductance, L_3, is 0.002 microhenry is used to monitor the discharge current.

Fig. 5B is a typical current waveform and shows that the circuit is very nearly critically damped and that the energy is almost completely dissipated in fifty microseconds. In a critically damped circuit, the following equations apply:

1) $i = \frac{E}{L}\ te^{-\frac{Rt}{2L}}$

2) $i_p = 0.736\ \frac{E}{R}$,

3) $L = \frac{R^2C}{4}$, and

4) $t_p = \frac{R\ C}{2} = \frac{2L}{R}$

In Fig. 5B, the peak current is about 226,000 amperes and the initial voltage is 19,200 volts. Solving Eqn. (2) for R_1 gives a value of 0.0625 ohm. The value for L_2 obtained from Eqn. (3) is 0.23 microhenry. It is noted that the calculated time required to reach peak current is 7.3 microseconds compared to an actual value of about 12 microseconds. This discrepancy can be accounted for by considering that the inductance is initially higher than the calculated value due to the concentration of current near the driver axis. As the plasma expands, the driver inductance decreases causing the current to reach a peak sooner than it would have

in the initially underdamped circuit, but later than for a critically damped circuit. The current waveform also shows a peaking effect which is apparently a distortion introduced by the inductance of the shunt. The fact that the total circuit inductance is decreasing during the first several microseconds of the discharge results in a higher rate of change of current as the peak value is approached than would normally be the case. The product of this rate of change and the inductance of the shunt is added to the shunt iR drop to give the output voltage and causes the shunt output to be higher during the current rise than during the decay which takes place at a much slower rate. Another way of describing the peaking effect is as an inductive overshoot due to the self-inductance of the shunt.

The current waveform is important in several respects. It shows that all of the energy is put into the driver gas before the diaphragm opening time of about 200 microseconds. The fact that there is no capacitor voltage reversal is beneficial in maximizing capacitor lifetime since the capacitors used are not designed for oscillatory discharge service. It should be noted that current waveforms for higher initial helium pressure do not show any significant differences from Fig. 5B.

The simplest means for measuring driver performance is to monitor the final driver pressure; however, it was found that holes in the Lexan liners shortened their life to one or, at best, two runs with questionable repeatibility of the arcing process. Therefore, it was decided to conduct the driver study mainly through the measurement of shock velocities in a short driven tube section (Fig. 4). Shock wave velocities and initial tube pressure measurements are thus used to infer driver conditions through a comparison with calculated shock tube performance parameters. This gives an indirect measure of driver performance properties such as pressure and temperature. The adequacy of this indirect technique of determining driver properties is discussed in later sections. An advantage of this approach is that it allows the concurrent investigation of problems such as diaphragm performance, shock wave attenuation, electrical effects on instrumentation response, and shock tunnel starting processes. A photograph of the prototype tube showing the major components is shown in Fig. 6.

The diaphragms separating the driver and driven tube are made of stainless steel (3/32" thick for maximum energy) and are scribed along two orthogonal diameters to a controlled depth (generally 20% - 40% of the thickness). It has been found that they open cleanly with negligible loss of material to the flow for all conditions studied to date. Probably because of the much more rapid pressure build-up, the diaphragms open at a considerably lower driver pressure than they do with combustion drivers.

Because of the high values of current involved in the operation of the electrically heated driver, considerable care must be exercised in avoiding ground loops in the instrumentation circuits. The only ground in the discharge circuit is at the diaphragm flange. Instrumentation grounds are also returned to tnis point via the driven tube.

DRIVER PERFORMANCE

Experimental data were obtained to determine typical performance characteristics for the arc heated helium driver described in the previous section. Figs. 7, 8, 9, 10 and 11 show interpretations of the basic data in terms of electrical energy conversion, driver pressure and temperature levels, and shock Mach number performance of the complete tube and power supply unit. Except were noted, these results are inferred from measured shock velocities, at a station towards the end of the driven tube, initial pressure levels, and ideal shock tube calculations (assuming air in thermochemical equilibrium).

Driver efficiency data results are presented in Fig. 7. These were obtained at an initial driver pressure, P_i, of 11.9 atm. Results are given both in terms of efficiency defined as the energy absorbed by the gas, Q_4, ratioed to the actual electrical energy supplied to the gas, Q_i, and in terms of Q_4 ratioed to the maximum or total available electrical energy (Q max = 47,000 joules based on the rated capacitor load). On the basis of Q_4/Q_i, peak efficiency occurs in the region of Q_i = 28,000 joules. The data also show that the driver gas never absorbs more than 50% of the maximum available electrical energy at the P_i level shown. When more than 60% of Q max (i.e., 28,200 joules) is supplied to the helium, the gas apparently reaches an energy saturation level below this 50% level.

Increasing P_i gives a considerable increase in efficiency as shown in Fig. 8. These results were obtained at maximum input energy (Q_i = Q max). However, the actual energy density in the helium, as indicated by T_4, decreases somewhat with increased P_i. At low values of P_i, only a small portion of Q_i is absorbed by the total mass of helium, although the T_4 level is high. At the high P_i levels, on the other hand, the electrical conversion efficiency apparently approaches 100%. The inferred P4 and T_4 values in the driver are plotted against P_i in Fig. 9. The scatter in the data points is partially caused by the spread of output energy levels for the various symbols. This figure suggests that at the high energy levels an approximate driver gas temperature range of 5000° to 6500° K is available at Q max as the P_i level is varied from 5 to 30 atmospheres.

The results of the previous three figures show the levels of energy conversion efficiency and gas properties that have been obtained in the prototype shock tube driver. These are useful results; however, if one is interested in maximizing shock tube performance in terms of shock velocity, the data should be presented against shock velocity or M_s. This is done for one P_1 level and at Q max in Fig. 10. The curve is seen to be relatively shallow, with performance increasing with P_i to an apparent maximum in the 25 to 30 atm. range. This slowly increasing performance with rapidly increasing efficiency is expected since, for example, at the low P_i values, the P_4/P_1 ratio is low but the T_4 level is high. The shallowness of the curve is an important characteristic because it allows operation over a range of effective driver temperature levels without a serious

sacrifice of shock velocity performance. This provides an interesting range of tailored conditions for shock tunnel operation (see Fig. 3).

As stated earlier, the general driver performance results discussed in this section were inferred from shock velocity measurements. These were generally taken approximately 10' from the diaphragm station. A few driver efficiency values were also determined for pressure measurements taken with piezoelectric gages located in the driver walls and these are shown in Fig. 8. As expected higher efficiency values are indicated by the pressure measurements. The difference between the levels shown could be explained by a shock wave attenuative rate of about 1.2%/ft which is consistent with the attenuation data given in Fig. 12. This value is about 1.6 times the value obtained for cold helium drivers at M_s values of the order of 7 as reported by Jones (17). Thus, while the difference in efficiency might be caused by attenuation effects, it may also represent in part a measure of the inaccuracies introduced by the assumption that the driver static properties can be obtained through shock velocity measurements.

The T_4 levels suggested by the P_4 measurements are shown in Fig. 8. These are considerably higher than those given by the M_s measurements. This point will be discussed later. Unfortunately, it has not yet been possible to obtain direct P_4 measurements at a P_i value of over 17 atmospheres where the high M_s efficiency data were obtained.

Fig. 11 presents a summary of shock Mach number performance that has been obtained with the prototype shock tube. Also shown is a theoretical prediction of M_s using a combustion driver at a final pressure of 4000 psi. This prediction does not include attenuation effects; therefore, the actual improvement in performance is even larger than shown on this plot.

Two other aspects of tube performance are illustrated in Figs. 12 and 13. Incident shock wave attenuation at three different shock velocity levels is shown in Fig. 12. At velocities of the order of 20,000 ft/sec the attenuation is found to be small, corresponding roughly to about .5%/ft. At the high velocity level, the attenuation is very severe. For the intermediate case shown in Fig. 12 the attenuation is approximately 1.5%/ft. Wall pressure histories behind the incident shock wave for an approximate range of M_s values of 14 to 25 are given in Fig. 13. A strong pressure rise such as that usually associated with wall boundary layer growth and shock wave attenuation (see reference 18) is seen in the higher M_s cases. It is interesting to note that the passage of the test air takes less than 50 μs in the prototype facility for most flows of interest. It is assumed that this relatively good attenuation and P_2 performance is due to the high P_1 levels (small boundary layer growth) at which high M_s values can be obtained. However, while the driver is capable of producing shock waves of well over 40,000 ft/sec (Fig. 12) the strong attenuation effects there probably preclude the conduction of meaningful tests in a facility of the dimensions of the prototype tube. This suggests a design of the type considered in Fig. 2 where the driven tube cross-sectional area is

several times that of the driver tube. Lin and Fyfe (20) have obtained very little attenuation effects in a tube of this type at M_s value of about 20 and at $P_1 = 20\,\mu$ Hg.

Calculations based upon a T_4 value of 5000° K have been made to determine the time of arrival at the pressure gage station of the reflected head of the driver expansion wave. (The arrival of the tail of the expansion wave is not important for the conditions of interest here.) This time is shown on each pressure record in Fig. 13. It is interesting to observe that the apparent arrival of the reflected head is significantly later than predicted. As yet no explanation has been found for this discrepancy between experiment and theory; however, it is in general agreement with the trend found by Holder and Schultz when they reduced the driver tube length in a cold hydrogen driven shock tube (19).

TEST CONFIGURATIONS

The previous section described the performance of the prototype shock tube with emphasis on the properties of the driver gas. In this section we will describe studies that relate to the conduction of experiments in two types of test configurations: model tests in the driven gas behind the incident shock wave and tests in the reflected shock tunnel configuration.

A. Straight Tube Test Configuration

As discussed in the last section, high M_s values were obtained in the prototype tube. An investigation was made to determine whether meaningful stagnation point heat transfer measurements could be made in the facility of the relatively small size of the prototype unit. Fig. 13 shows a sketch of the shock tube model test configuration in the prototype facility and the wave diagram for the test flow. The actual quasi-steady test time is somewhat less than the test time shown because of the necessity for starting the flow around the test model. A hemispherical model 3/4" in diameter was located as shown in the figure. This model was instrumented at its stagnation point with either of two types of heat transfer gages; a thick film, or calorimeter, gage (3) or a thin film heat transfer gage (21). Pressure gages were located so that shock velocity measurements could be made just upstream of the model. In addition, the stagnation region shock layer near the model was observed with an optical pyrometer. The purpose of the pyrometer was to give an indication of the steadiness of luminosity generated by the stagnation region shock layer flow.

Tests were run to determine the stagnation point heat transfer in air over a relatively wide range of stagnation enthalpy levels. Although the duration of steady flow at the nose of the model was quite short, it was of sufficient duration to allow measurement of the heat transfer rates. Typical data taken at approximately the same shock Mach number are shown in Fig. 15 (the thin film and pyrometer data were taken on the same run). Note that the grids have been

displaced to coincide with the arrival of the incident shock wave. The three records are in general agreement concerning the existence of a finite test time which is approximately 10 μs long. The flow starting time is 3 to 5 μs . The apparent end of the test occurs at 50 to 60% of the predicted theoretical test time which is in general agreement with other investigations (e.g., see reference 22). The calorimeter gage shows some interesting effects. These gages were not provided with an insulation coating. They indicate an apparent reduction in resistance a few μs before the arrival of the incident wave. This is interpreted (without serious justification at present) either as the arriv l at the gage, or the approach towards it, of high energy electrons that have migrated ahead of the incident wave, or as a photoelectric current generated by high energy radiation from the shock heated air behind the incident wave. After its arrival there is a rapid adjustment of the flow, and of the gage response, and the establishment of the steady state test time during which the gage reads the convective heat transfer (indicated by the linear gage response). Since the stagnation region pressure level is quite high (the order of 20 atmospheres) the boundary layer is probably in equilibrium, and thus the gage is insulated from the relatively highly ionized shock layer flow. The thin film platinum gages were coated with a thin evaporated layer of SiO (less than . 1 μ thick) which appears to have insulated the gage from the early electrical effects observed with the calorimeter gages. However, it is noted that the output signal of the thin film gage is approximately 2 orders of magnitude greater than that of the calorimeter, so that the observed extraneous electrical signals could be lost in the noise level of the circuit. The gage response is as expected during the apparent test time; however, the surface temperature change during this time is quite high (approximately 350° K) so that the substrate properties can change significantly and cause uncertainties in the measured heating rate. A correction factor for this effect, as suggested by Hartunian (23), has been applied to the thin film data. Because of this effect and since the thin film gages have often ruptured during test time -- notice the apparent discontinuity in response in Fig. 15 -- the thin film data was used primarily to provide qualitative support for the calorimeter gage data. The pyrometer data were also interpreted only qualitatively to support the existence of a relatively steady test time of reasonable duration. The relatively small fluctuations in radiant intensity from the shock layer seen in Fig. 15 are assumed to be caused by much smaller amplitude oscillations in thermodynamic properties of the flow.

Early heat transfer measurements in the prototype tube (presented as preliminary data in Fig. 17) were complicated by the existence of extraneous electrical effects in the apparent data when displayed on an oscilloscope. It was possible to reduce these effects to acceptable levels by the common grounding of the instrument circuits with the driver circuit, as discussed earlier, and by feeding the gage output through a balanced differential amplifier. This latter procedure eliminates the extraneous gage signals caused by effects that give a charge flow distributed over the surface of the gage. The steps in the process are as follows. The differential amplifier is connected across the active gage leads. Each leg of the amplifier has a 1 megohm resistance to ground. A square wave pulse of the same

magnitude as that of the extraneous signal observed during the test is impressed across the gage leads and the legs of the amplifier are balanced to eliminate the signal after the initial pulse. The pulse is caused by the capacitance to ground on each leg of the differential amplifier and has a rise time of approximately 3 μs, which is comparable to the flow starting time as interpreted from Fig. 15. This balancing technique has been checked at the test conditions of interest. The battery supplying current to the gage circuit was shorted (no gage current, and, therefore, no measure of the resistance change of the gage due to heating) and a test was run. This resulted in a signal of the following type:

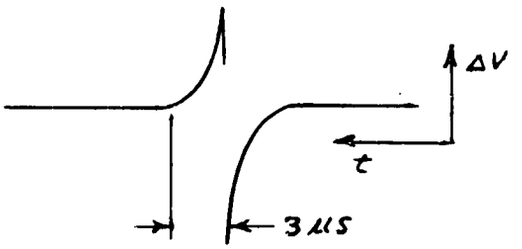

Thus, it appears that after approximately 3 μs the gage will be free to respond accurately to direct heating from the gas. On the basis of this technique and on the assumption that there is no gage shorting due to a conducting layer near the gage surface, it is concluded that the typical response of the calorimeter gage during the indicated test time is caused by heat transfer to the gage surface, the quantity it is desired to measure. Notice that gage shorting by the gas, if it existed, would result in a reduction of the heating rate inferred from the gage signal.

It has been found that satisfactory heat transfer records can be obtained in the present facility to M_s levels of approximately 26 (simulated flight velocity of 40,000 ft/sec). Above this value, data are difficult to interpret. This may be due to the short test times available and strong incident shock wave attenuation, which are, at least in part, caused by the low P_1 values required to go to higher M_s levels, or to an increase in importance of the electrical effects generated by the plasma. It is probable that, with the advent of larger scale facilities and with improvements in instrumentation sensors, this upper limit will be extended appreciably.

No direct measure of equilibrium in the test gas was attempted during this program. It was assumed that the relatively high pressures of the test would establish equilibrium conditions very quickly in the test gas. This assumption is supported by the relative steadiness of the pyrometer records during the apparent test time and by data given in reference 24.

Stagnation point heat transfer data were obtained through high stagnation enthalpy levels and at relatively high pressure levels; thus, the possibility that radiation from the hot gas shock layer to the body could add to the measured heat transfer rate must be considered, even for the small dimensions of the test model. The m agnitude of this effect was calculated using the emissivity data of Breene and Nardone (25). The maximum stagnation point radiative heating rates (assuming complete absorption by the highly reflecting heat transfer gages) for several P_1 levels (including those investigated -- 1, 5 and 25 mm Hg) are shown in Fig. 16. Since the measured heating rates at $M_s = 25.6$ and $P_1 = 1$ mm Hg were over 100,000 BTU/ft^2-sec, it is seen that the predicted radiation level is below 10% of the measured value or less if we consider the gage reflectivity. Also shown in Fig. 17 are curves presented by Rose (26) which were calculated based on the emissivity data of Kivel and Bailey (27). These results do not substantially differ from the Breene and Nardone results in the regions of interest. It appears reasonable to conclude that the observed data are essentially caused by the convective mechanism. It is planned to evaluate this conclusion in the near future through actual radiative heating measurements.

Fig. 17 shows several stagnation point convective heat transfer data obtained in the shock tube. These data extend through an M_s level of 25.6 or to a simulated flight velocity of about 39,000 ft/sec. There is seen to be good agreement with the theoretical predictions of Scala which include ionization effects. The data shown in this curve represent extensions of results discussed in reference 28.

B. Shock Tunnel Test Configuration

Some of the characteristics of a reflected shock tunnel using an electrically heated driver will be discussed in this section. Fig. 18 shows a representative wave diagram for the shock tube portion of a shock tunnel facility. It is assumed that the tailored interface condition has been achieved; that is, there is no downstream reflection from the point of intersection of the reflected shock wave and the contact front. The nozzle flow time (nozzle starting time will not be considered here) can be limited by one of three events in the usual shock tunnel design: first, the driver gas processed by both the incident and reflected shock waves can be exhausted; the other two limits that could occur, are the arrival at the nozzle station of either the tail or reflected head of the expansion wave generated by the diaphragm opening process. Depending upon the design of the facility, any one of these processes could cause termination of the useful nozzle flow. The reflected shock wave could also influence the test flow; however, this will not usually occur unless a constriction at the diaphragm station is incorporated into the design (the steady tailored configuration --(see reference 10).

Test time limitations are important, since the power supply can be relatively expensive if a long driver is needed, and since there may be physical limitations upon the length of driver in which a satisfactory uniform axial discharge can be generated. Calculations for typical test time limits are given in Fig. 19. If the driver tube length is small with respect to the length of the driven

tube, the reflected head of the expansion wave appears to be a serious limitation; thus, we must consider the use of high L_1/L values. Because of the concern about the total driver length; however, we may be restricted to a relatively short driven tube. To illustrate the type of facility that appears to be feasible based upon a moderate extrapolation of the present developments, consider the example of a 15' long, 2" id driven tube. We will obtain approximately .9 millisecond of test time at $M_s = 16$ if we have a driver tube length of 7.5'. A throat diameter of 5/16 to 3/8" would probably be feasible here, considering the test gas lost in the contact zone. This would allow a test section diameter of 2' to 3' at reasonable A/A^* values (order of 10^4). A facility with such nominal characteristics appears to be attractive, since a nozzle flow time of about 1 millisecond would be reasonable for several types of experiments, particularly in the higher enthalpy ranges where the nozzle starting time will be relatively short.

The limitation imposed by the loss of energy by radiation from the hot gas in the reflected region should also be considered. Fig. 20 shows the time required for the Region 5 air to lose approximately 20% of its internal energy by radiation to its surroundings (assuming complete loss of the radiated energy). If we desire to work in the P_1 range of .01 to .1 atmosphere and consider the 20% drop to be acceptable we are, therefore, limited to M_s levels of about 18 for flow durations of the order of 1 millisecond.

A few data were obtained to determine whether tailoring conditions were obtainable at the high M_s values indicated by the driver performance study described earlier. Using a P_i value of 12 atmospheres and Q max, several pressure histories were measured on the tube end wall in the configuration shown in Fig. 4. Three of these are shown in Fig. 21. The data of Fig. 8 suggest that the T_4 value for the chosen driver condition lies between 5500 and 7000° K, and the P_5 results indicate that tailoring is achieved in the vicinity of $M_s = 20$. From the horizontal scales in Fig. 19 it can be seen that this tailored M_s value corresponds to a T_4 value of approximately 6800° K. Therefore, this result indicates that the effective driver temperature obtained in the prototype is more closely predicted by the driver pressure measurements than by the shock velocities. This is expected, of course, and is in agreement with the attenuation results discussed earlier. The lower record in Fig. 21 shows that the equilibrium interface condition (19) is reached (at least for that M_s value) approximately 200 μs after shock reflection. Therefore, if desired, this method of operation could be employed to extend the long time, high M_s capabilities of such a facility, although this entails calculation (and its attendent assumptions) of the "steady" pressure level through a series of wave interactions (19).

One other interesting result is seen in Fig. 21. The theoretically predicted arrival of the reflected head of the driver expansion wave is shown on the $M_s = 20.2$ data. As for the region 2 records, the actual time to arrival appears to be about twice the theoretical value. This result is important, since it indicates that the

reflected heat time limitations shown in Fig. 19 can be delayed. That is, the driver tube for a particular driver length can be considerably shorter (a factor of 2 is suggested by the present limited data) without restricting the available test time. By the same reasoning, the driven tube can be longer for a given driver length.

CONCLUSIONS

The feasibility of an arc heated helium driven shock tube has been established on a prototype scale. A considerable improvement in performance compared to more conventional shock tube driver techniques is available. This is exhibited, first, in the ability of the new shock tube to drive stronger shocks into higher pressure initial conditions than is now possible and, second, in the extension of tailored reflected shock tunnel operation conditions to high M_s levels. The desirability of the improved performance characteristics has been justified on the basis of the simulation of flight enthalpy and pressure levels for hypervelocity re-entry studies.

The performance of the arc heated driver has been characterized through the measurement (primarily by indirect methods) of gas properties and efficiencies. A wide range of operating conditions are available. The utility of a straight tube model test configuration on the prototype scale has been established, at least over an appreciable range of operating conditions, and some of the limitations of reflected shock tunnels (flow time, radiation losses) have been investigated.

It is believed that larger scale facilities of more experimental utility than the prototype may now be developed through the extrapolation of information gathered during this study.

ACKNOWLEDGEMENT

The author would like to acknowledge the following contributors to the present work: Messrs. J. Gruszczynski, R. Garvine, B. Lieu, and Miss B. Miller, who provided analytical support; Dr. S. Havriliak who conducted the early experimental studies; and M. Stelman, Mr. G. Kernicky and Miss B. Maguire who aided in the instrumentation development and operated the experimental equipment.

This work was supported in part by the USAF Ballistic Systems Division under Contract No. AF04-(647)-617.

NOMENCLATURE

Symbols

A -- area (also amperes)
C -- capacitance
D -- diameter
E -- volts
I -- radiant intensity
L -- length (also inductance)
M -- Mach number
P -- pressure
Q -- energy
R -- nose radius (also resistance)
T -- temperature
V -- voltage
X -- axial distance
d_* -- nozzle throat
h -- enthalpy
l -- length
$\dot{q}$ -- heat transfer rate
t -- time
u -- velocity

Subscripts

.8 -- 80% of initial h value
1 -- initial driven tube conditions (also electrical circuit)
2 -- behind normal shock (also electrical circuit)
3 -- behind contact surface (also electrical circuit)
4 -- final driver conditions
5 -- reflected region conditions
f -- flight conditions
N, o -- nose of model (heat transfer)
i, o -- initial conditions
s -- stagnation conditions (also shock)

REFERENCES

1. Resler, E. L., Lin, S. C., and Kantrowitz, A.; The Production of High Temperature Gases in Shock Tubes; JAP, Vol. 23, No. 12; December 1952.

2. Hollyer, R. N., Hunting, A. C., Laporte, O., and Turner, E. B.; Luminousity Generated by Shock Waves; Nature, 171, 395; 1953.

3. Rose, P. H., and Stark, W. I.; Stagnation Point Heat Transfer Measurements in Dissociated Air; Journal of Aero/Space Sciences; Vol. 25, No. 2, February 1958.

4. Rabinowicz, J.; Aerodynamic Studies in the Shock Tube; GALCIT, Hypersonic Res. Proj. Memo No. 38, June 1957.

5. Hertzberg, A., and Wittliff, C.; Studying Hypersonic Flight in the Shock Tunnel; IAS Paper 60-67, IAS Nat. Summer Ntg., Los Angeles, Calif.; June 1960.

6. Aronson, P. M., Marshall, T., Seigel, A. E., Slawsky, Z. I., and Smiley, E. F.; Shock Tube Wind Tunnel Research at the U. S. Naval Ordnance Lab., AFSWC Proceedings of 2nd Shock Tube Symposium; SWR-TM-57-2, February 1957.

7. Nagamatsu, H. T., Geiger, R. E., and Sheer, R. E.; Hypersonic Shock Tunnel; JARS, Vol. 29, No. 5; May 1959.

8. Kaegi, E. M., Warren, W. R., Harris, C. J., and Geiger, R. E.; The Capabilities of the Shock Tunnel in the Study of the Aerodynamics of Atmospheric Entry; ARS Paper No. 1554-60, ARS 15th Annual Meeting, Washington, D. C., December 1960.

9. Ziemer, R. W.; Extended Hypervelocity Gas Dynamic Charts for Equilibrium Air, STL TR-60-0000-09093, April 1960.

10. Witliff, C. E., Wilson, M. R., and Hertzberg, A.; The Tailored Interface Hypersonic Shock Tunnel, JA/SS, Vol. 26, No. 4; April 1959.

11. Holder, D. W., and Schultz, D. L.; On the Use of Shock Tunnels for Research on Hypersonic Flow; 2nd International Conference on the Aeronautical Sciences; Zurich, 1960.

12. Nagamatsu, H. T., Workman, J. B., and Sheer, R. E., Jr.; Hypersonic Nozzle Expansion of Air With Atom Recombination Present; JA/SS, Vol. 28, No. 11; November 1961.

13. Hall, J. G., Eschenroeder, A. Q., and Marrone, P. V.; Inviscid Hypersonic Air-Flows with Coupled Non-Equilibrium Processes; IAS Paper 62-67. IAS 30th Annual Mtg., New York, N. Y., January 1962.

14. Eschenroeder, A. Q.; Ionization Non-Equilibrium in Expanding Flows; ARS Journal; Vol. 32, No. 2; February 1962.

15. Fowler, R. G., Goldstein, J. S., and Clotfelter, B. E.; Luminous Fronts in Pulsed Gas Discharges; Physical Review, Vol. 82, No. 6; June 1951.

16. Kolb, A. C.; Magnetically Driven Shock Waves; Bul. Amer. Phys. Soc., Series II, Vol. 2, No. 1; January 1957.

17. Jones, J. J.; Experimental Invest. of Attenuation of Strong Shock Waves in Shock Tube with Hydrogen and Helium as Driver Gases; NACA TN 4072; 1957.

18. Wittliff, C. E., and Wilson, M. R.; Shock Tube Driver Techniques and Attenuation Measurements; CAL Report No. AD-1052-A-4; AFOSR TN-57-546; AD 136531; August 1957.

19. Holder, D. W., and Schultz, D. L.; The Duration and Properties of the Flow in a Hypersonic Shock Tunnel; Paper No. 1970-61, ARS-AFOSR International Hypersonics Conference, Cambridge, Mass., August 1961.

20. Lin, S. C., and Fyfe, W. I.; Low-Density Shock Tube for Chemical Kinetics Studies; Physics of Fluids, Vol. 4, No. 2; February, 1961.

21. Vidal, R. J.; Model Instrumentation Techniques for Heat Transfer and Force Measurements in a Hypersonic Shock Tunnel; CAL Report No. AD-917-A-1, WADC TN 56-315; February, 1956.

22. Hooker, W. J.; Testing Time and Contact-Zone Phenomena in Shock Tube-Flows; The Physics of Fluids, Vol. 4, No. 12; December, 1961.

23. Hartunian, R. A., and Varwig, R. L.; A Correction to Thin-Film Heat Transfer Measurements; AeroSpace Corp. Report, May, 1961.

24. Valentin, Pierre; Electrical Conductivity of Air Ionized by a Shock Wave; Proc. of French Academy of Sciences; July 10, 1961.

25. Breene, R. G., Jr., et al; Radiance of Species in High Temperature Air (3000° K - 25,000° K); GE MSVD, TIS Rep. No. R62SD23; February, 1962.

26. Rose, P. H.; Re-Entry from Lunar Missions; AVCO Ever. Res. Lab. AMP 69; December, 1961.

27. Kivel, B., and Bailey, K.; Tables of Radiation from High Temperature Air; AVCO Research Report 21; December, 1957.

28. Scala, S. M., and Warren, W. R.; Hypervelocity Stagnation Point Heat Transfer; JARS, Vol. 32, No. 1; January, 1962.

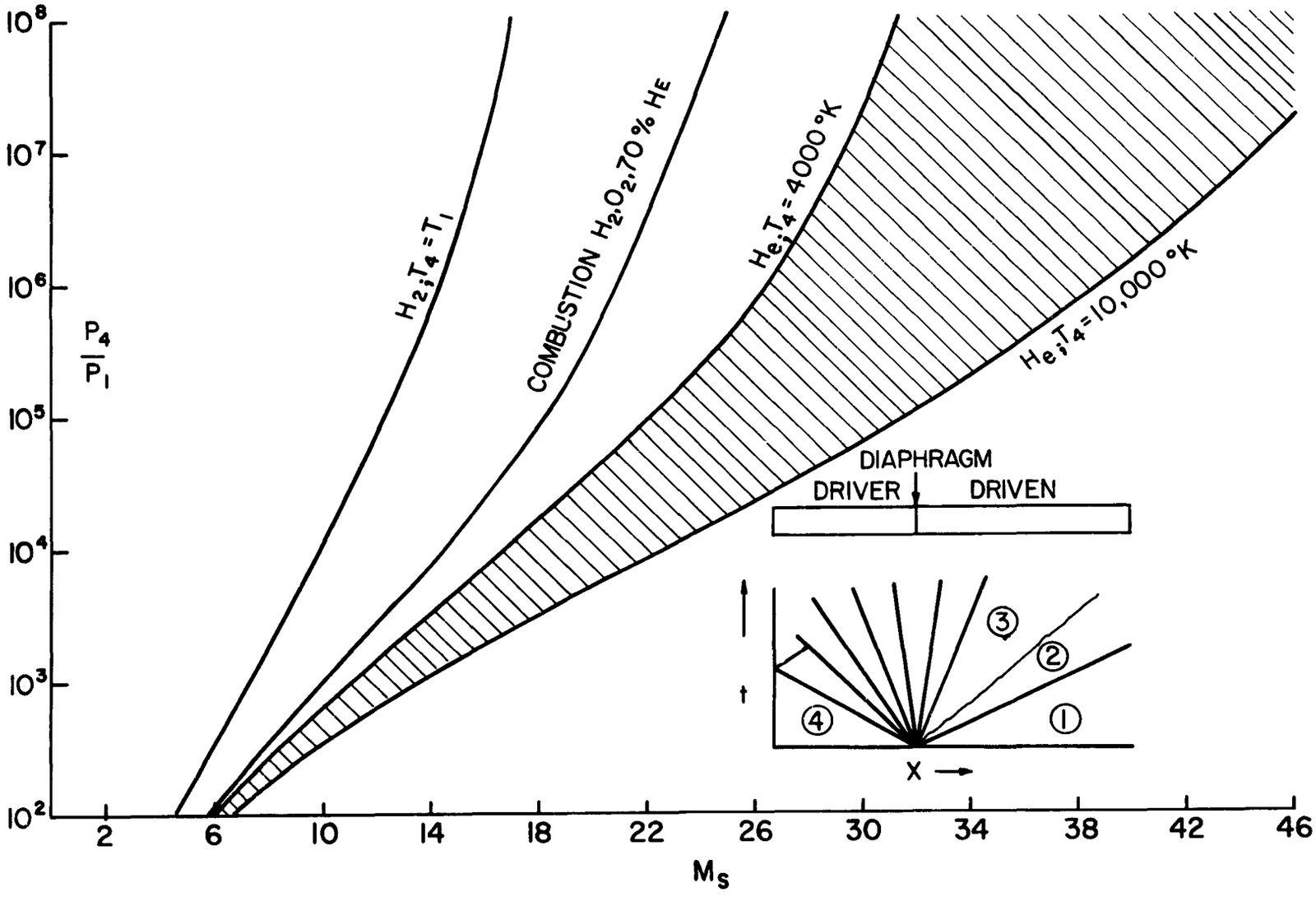

FIGURE 1 THEORETICAL PERFORMANCE OF AN AIR SHOCK TUBE WITH SEVERAL DRIVERS

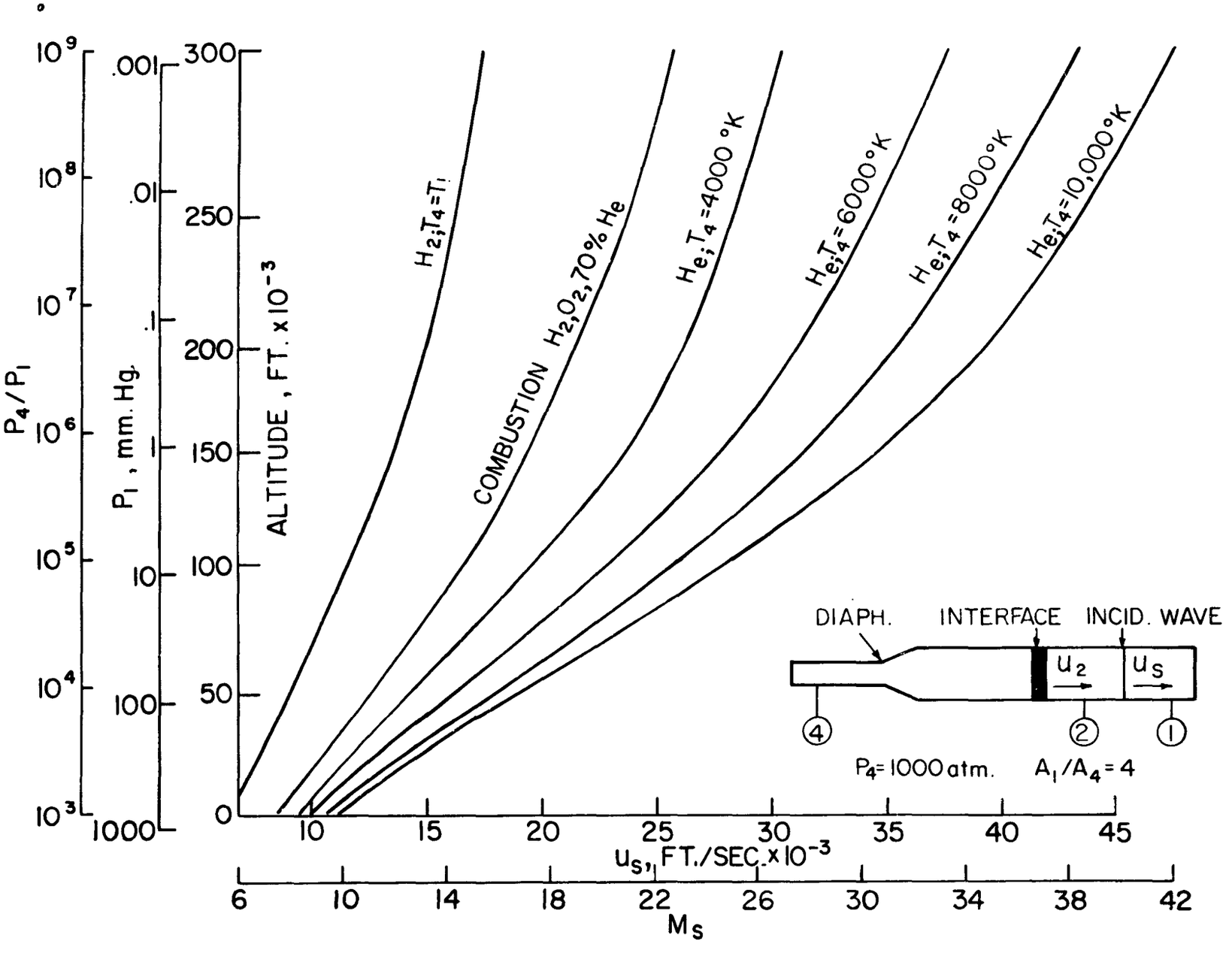

FIGURE 2 PERFORMANCE OF TYPICAL AIR SHOCK TUBE WITH SEVERAL DRIVERS

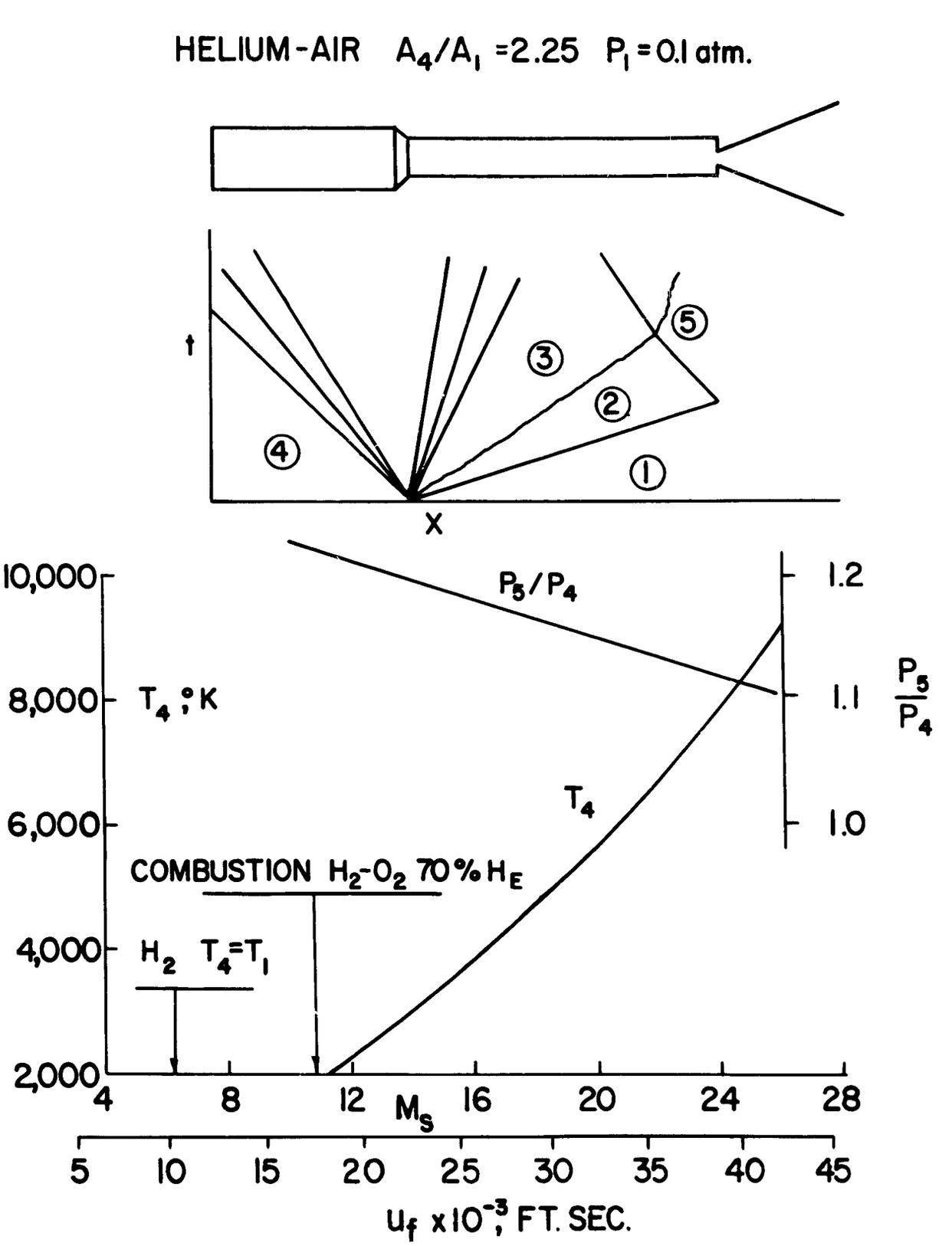

FIGURE 3 PERFORMANCE OF REFLECTED SHOCK TUNNEL TAILORED INTERFACE OPERATION

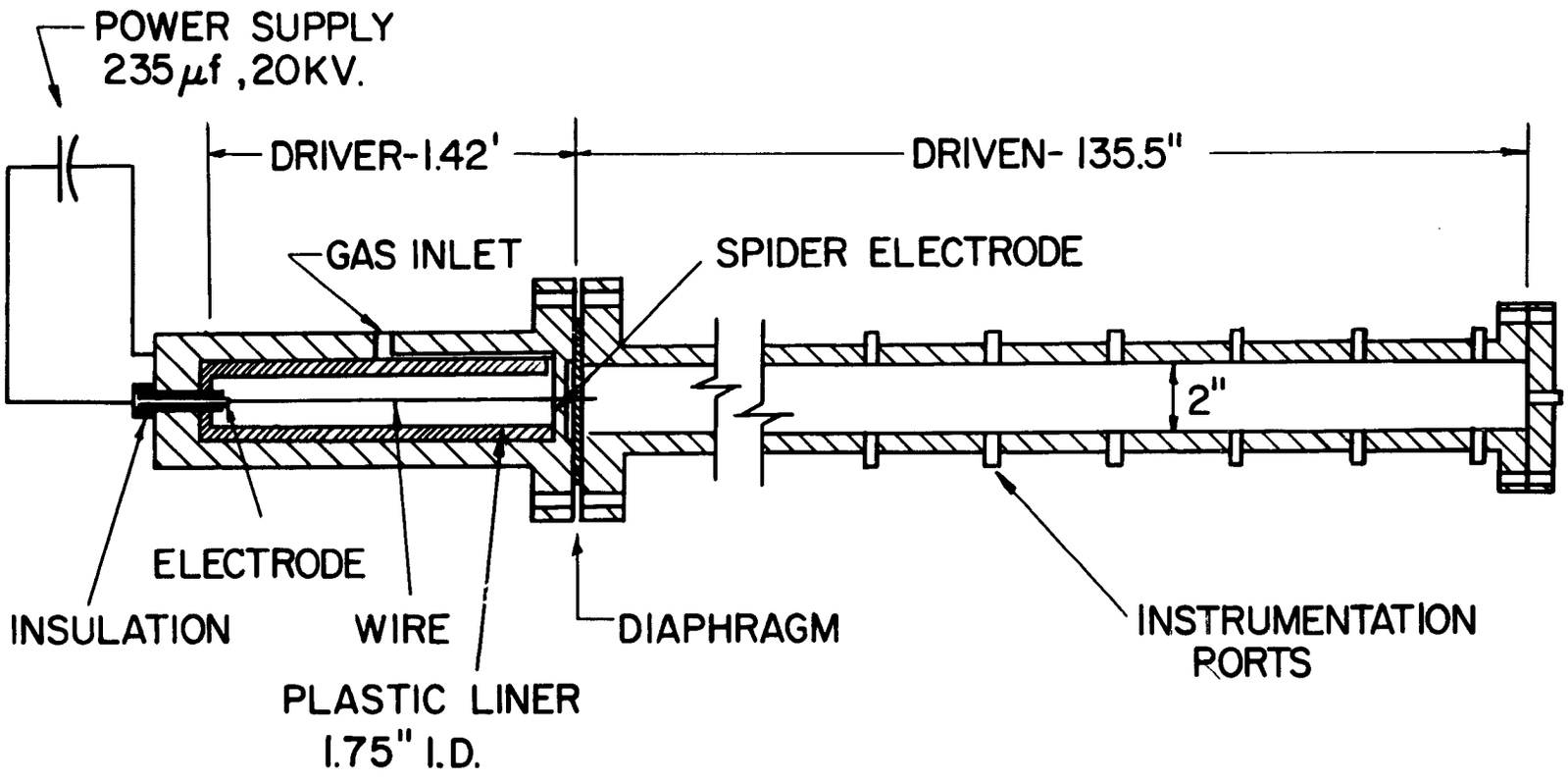

FIGURE 4 DESIGN OF ARC HEATED SHOCK TUBE

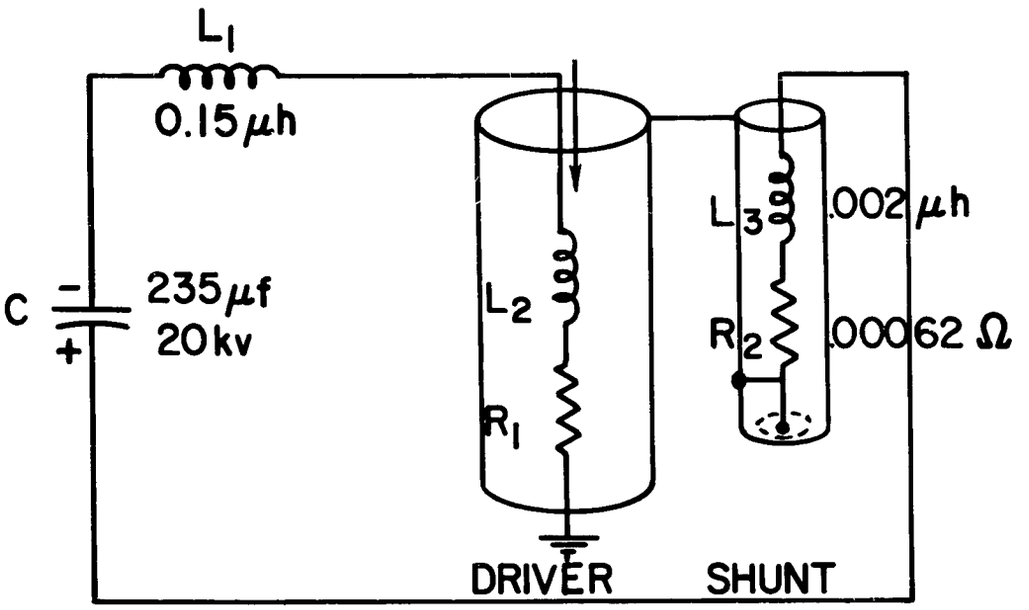

Figure 5a CIRCUIT DIAGRAM

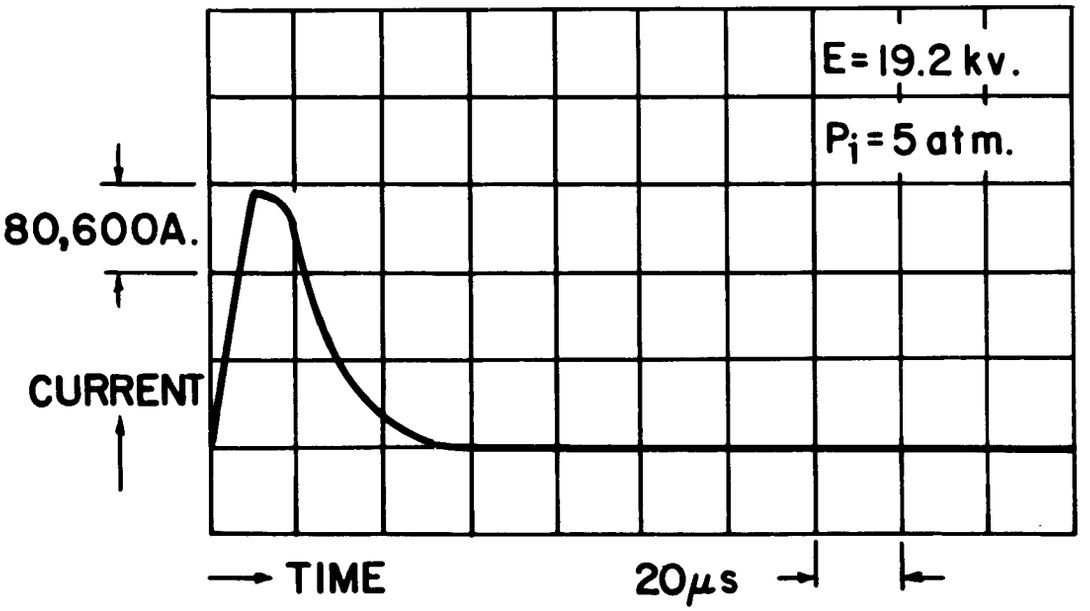

Figure 5b CURRENT WAVEFORM

FIGURE 5 TYPICAL ELECTRICAL CHARACTERISTICS
PROTOTYPE SHOCK TUBE

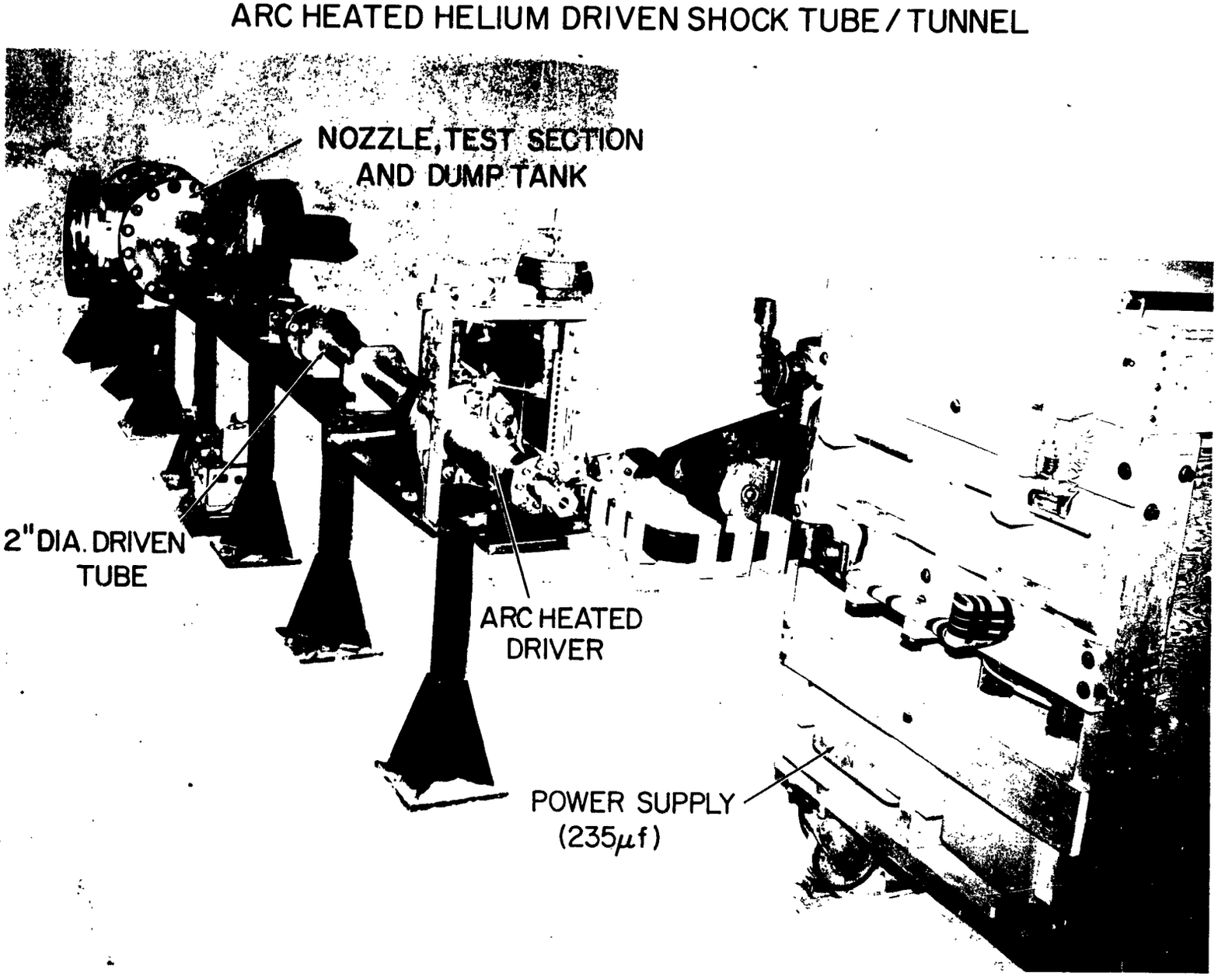

FIGURE 6 ARC HEATED HELIUM DRIVEN SHOCK TUBE/TUNNEL

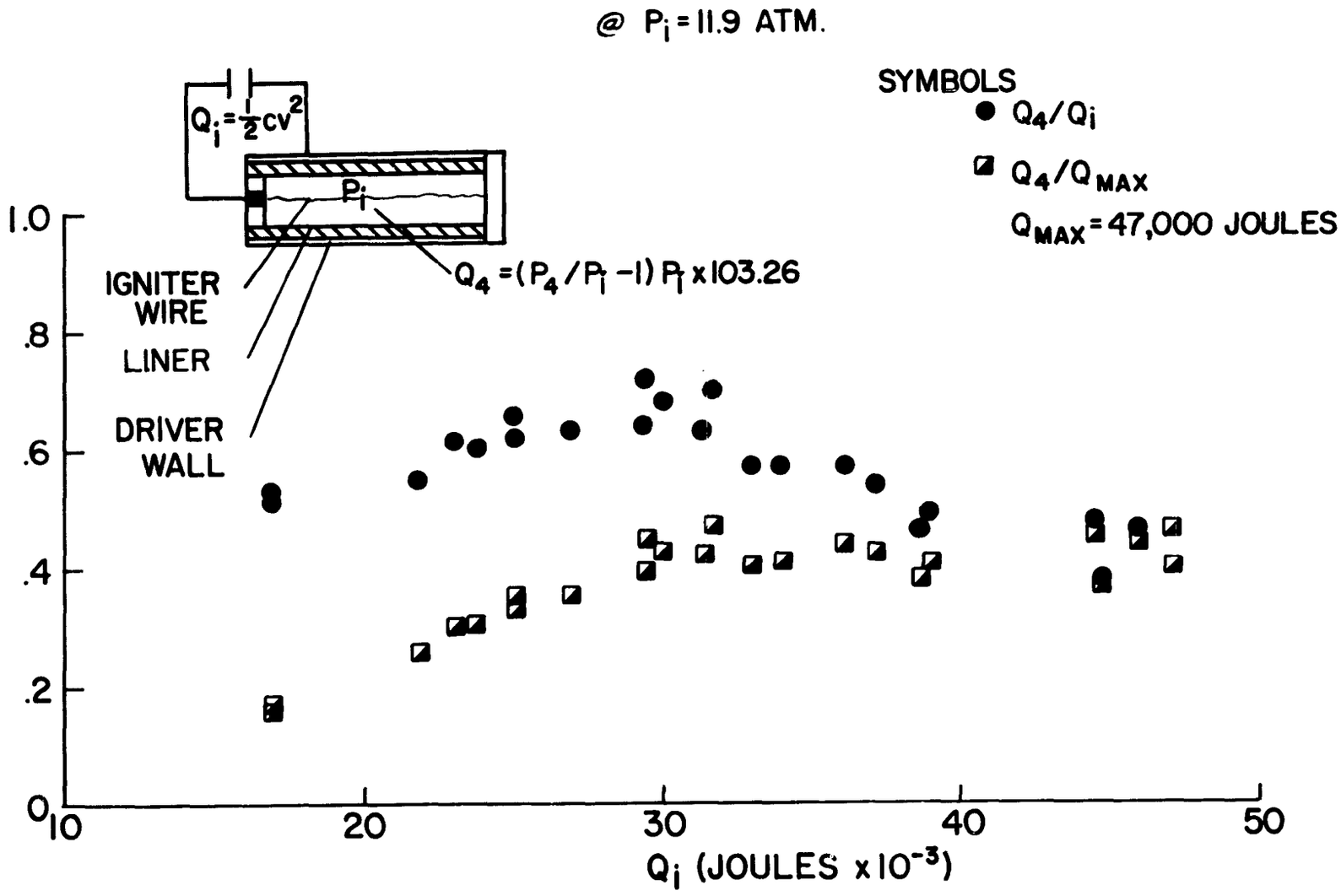

FIGURE 7 ARC HEATED DRIVER EFFICIENCY (HELIUM)

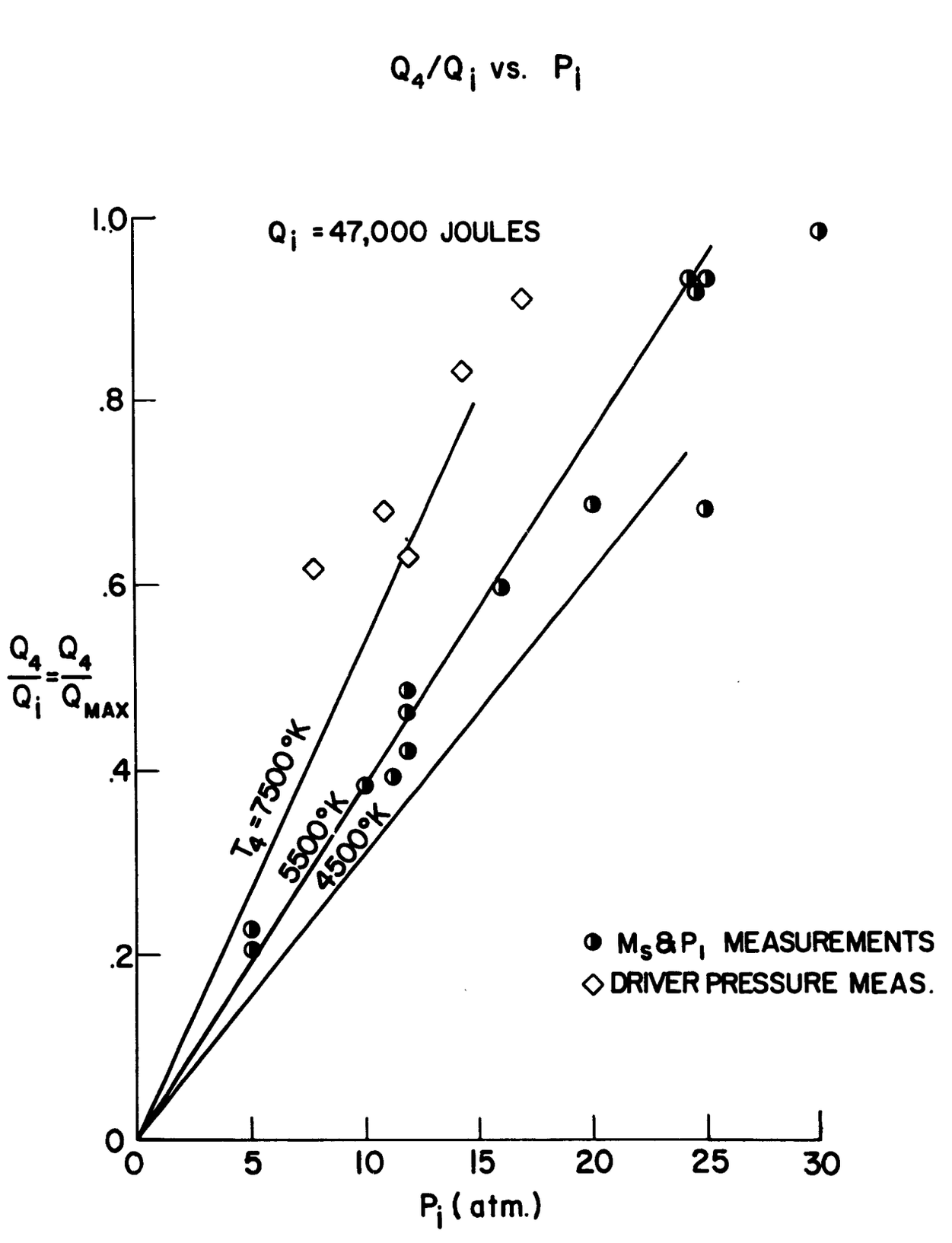

FIGURE 8 ARC HEATED HELIUM DRIVER EFFICIENCY

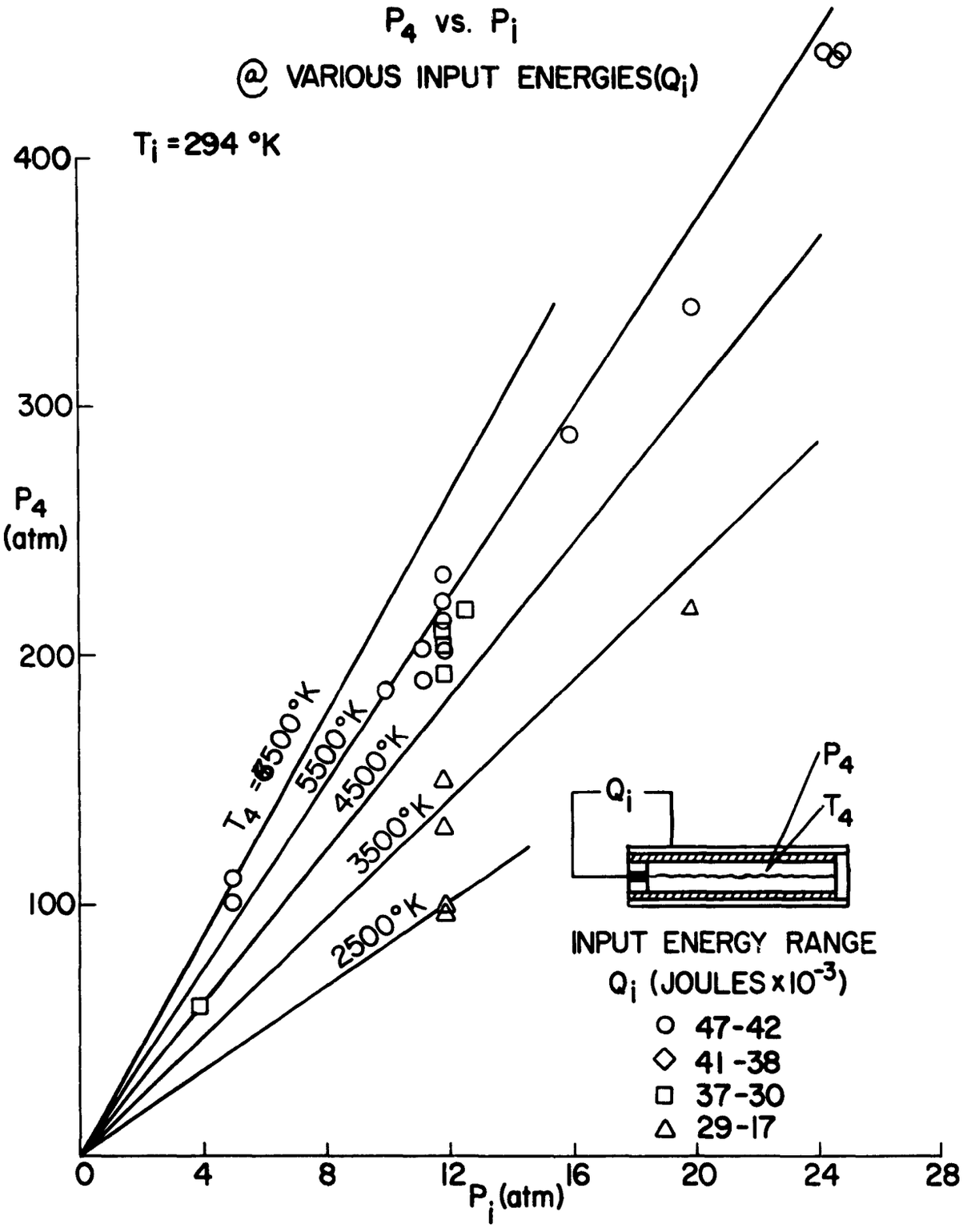

FIGURE 9 ARC HEATED HELIUM DRIVER PERFORMANCE

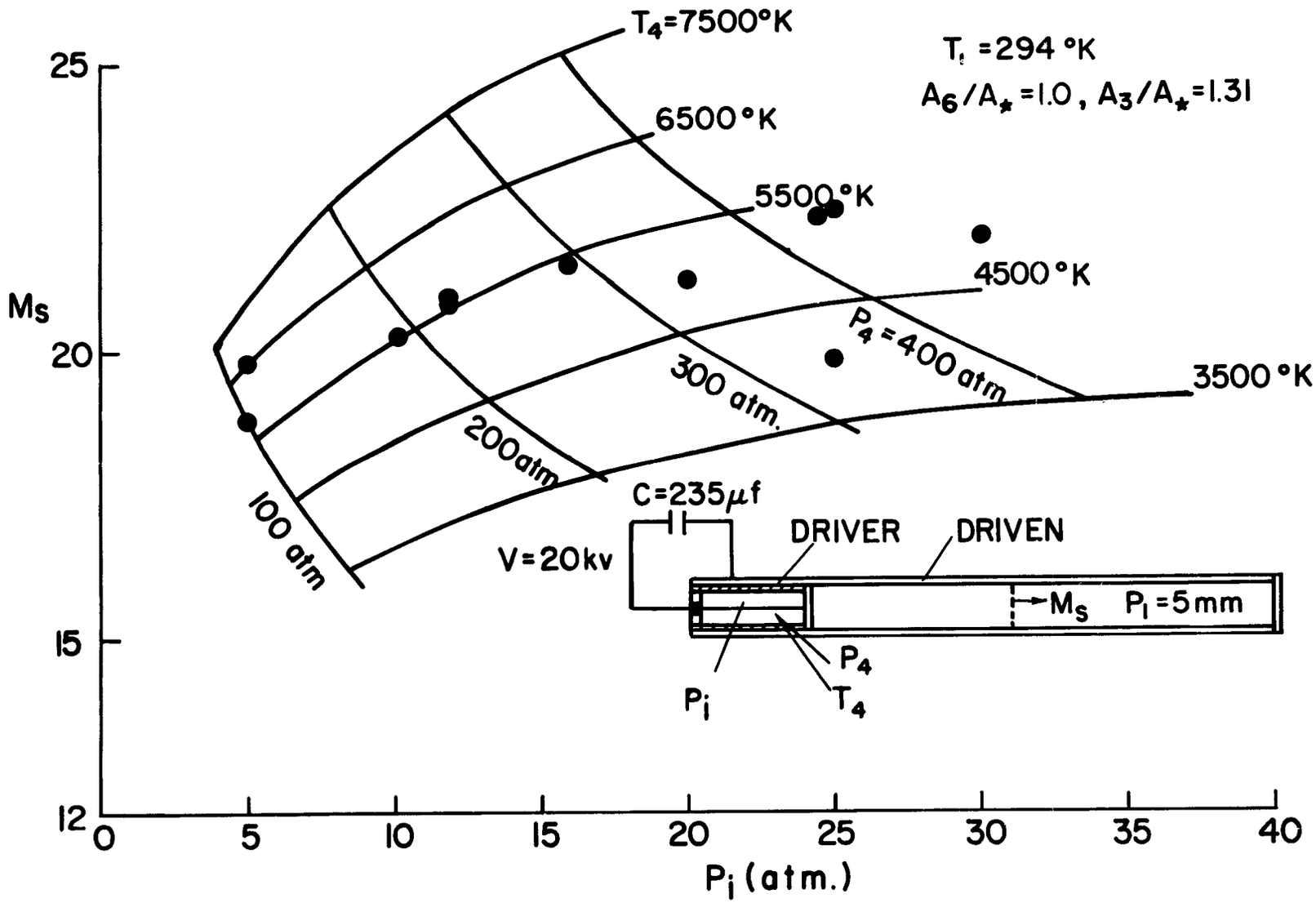

FIGURE 10 ARC HEATED HELIUM DRIVER; AIR-SHOCK TUBE PERFORMANCE (CONSTANT INPUT ENERGY - 47,000 JOULES).

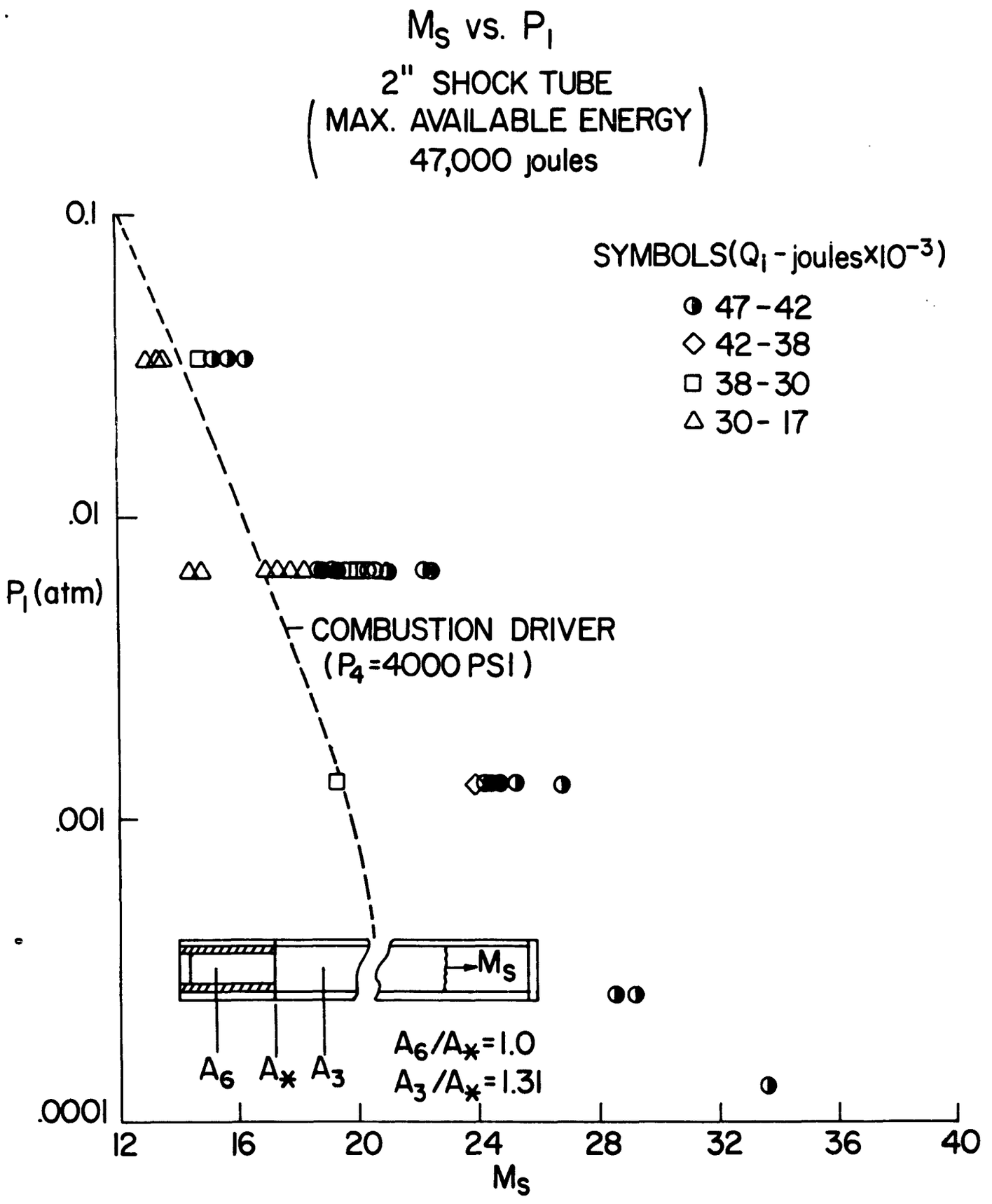

FIGURE 11 ARC HEATED HELIUM DRIVER SHOCK TUBE, M_S VS. P_1

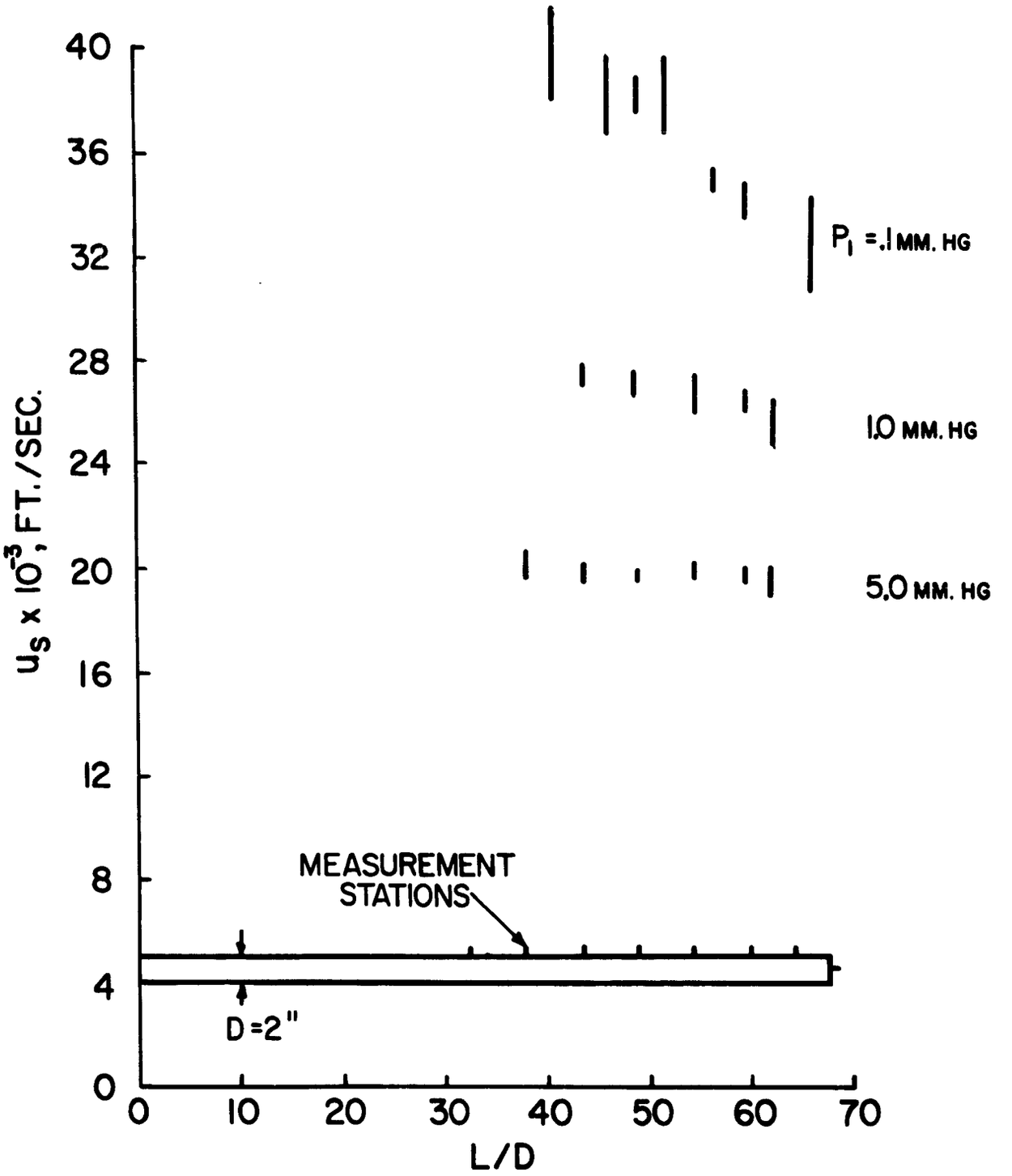

FIGURE 12 INCIDENT SHOCK WAVE ATTENUATION

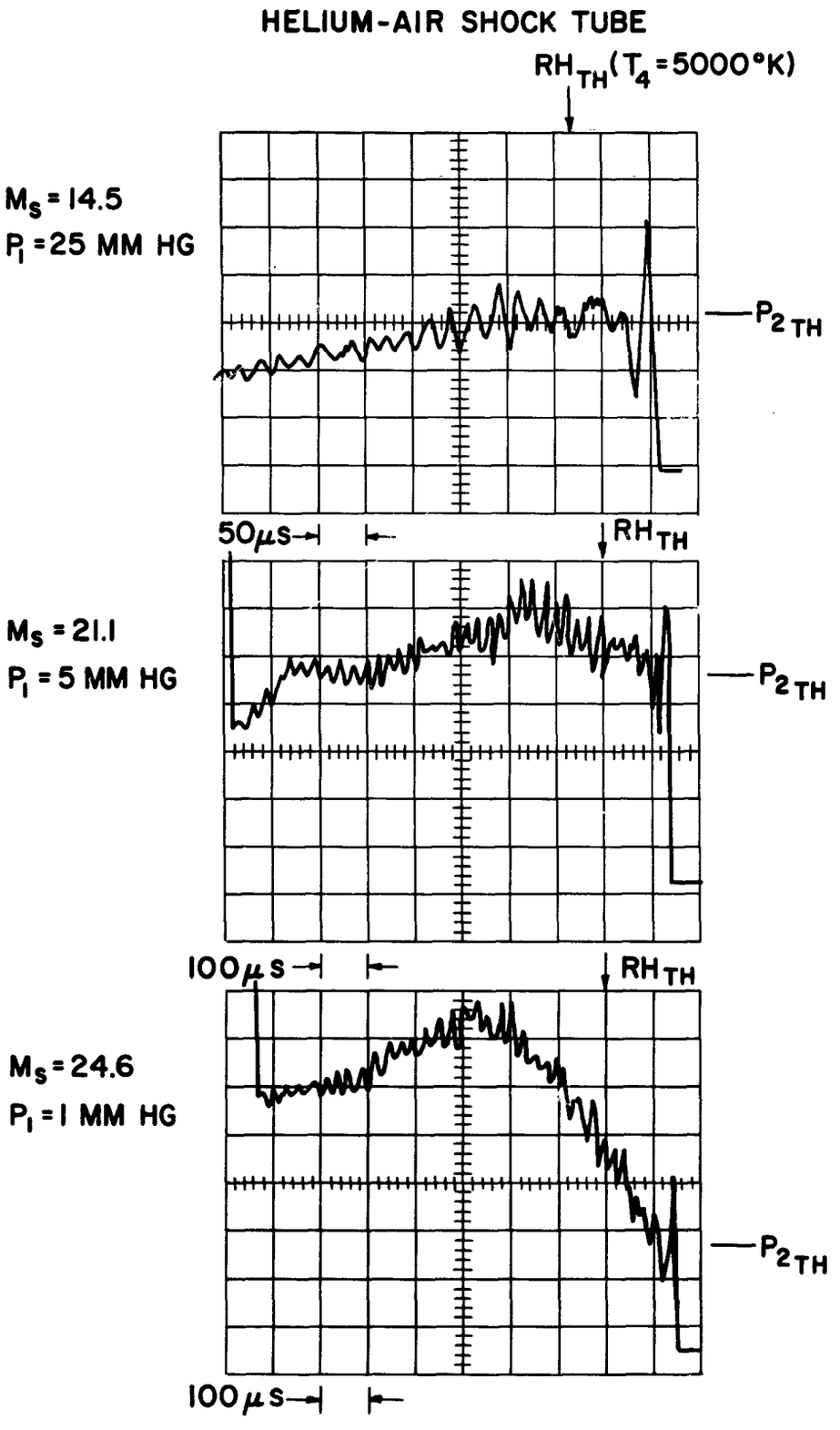

FIGURE 13 PRESSURE RECORDS BEHIND INCIDENT SHOCK WAVE

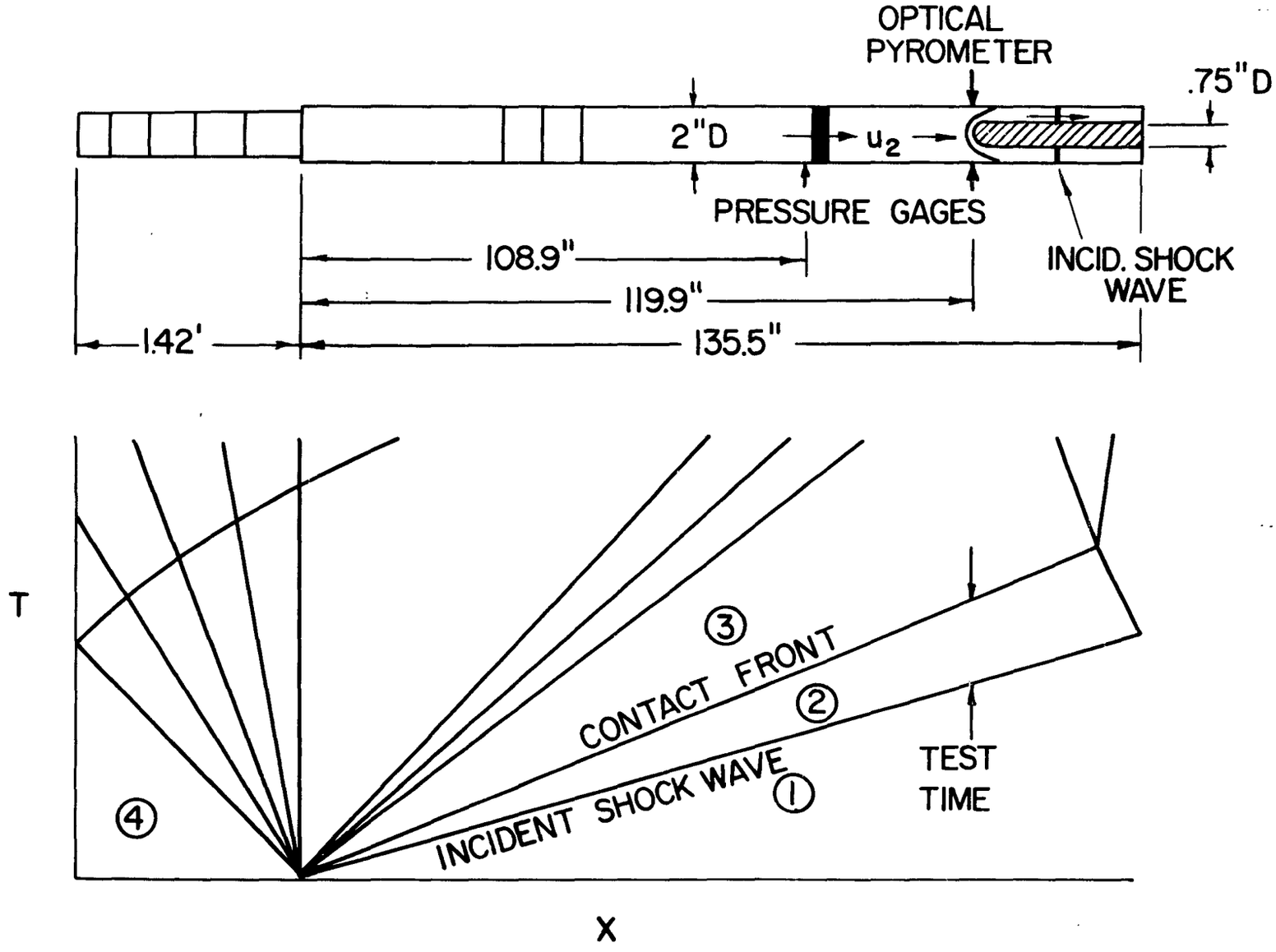

FIGURE 14 STRAIGHT TUBE TEST CONFIGURATION MODEL
HEAT TRANSFER MEASUREMENTS

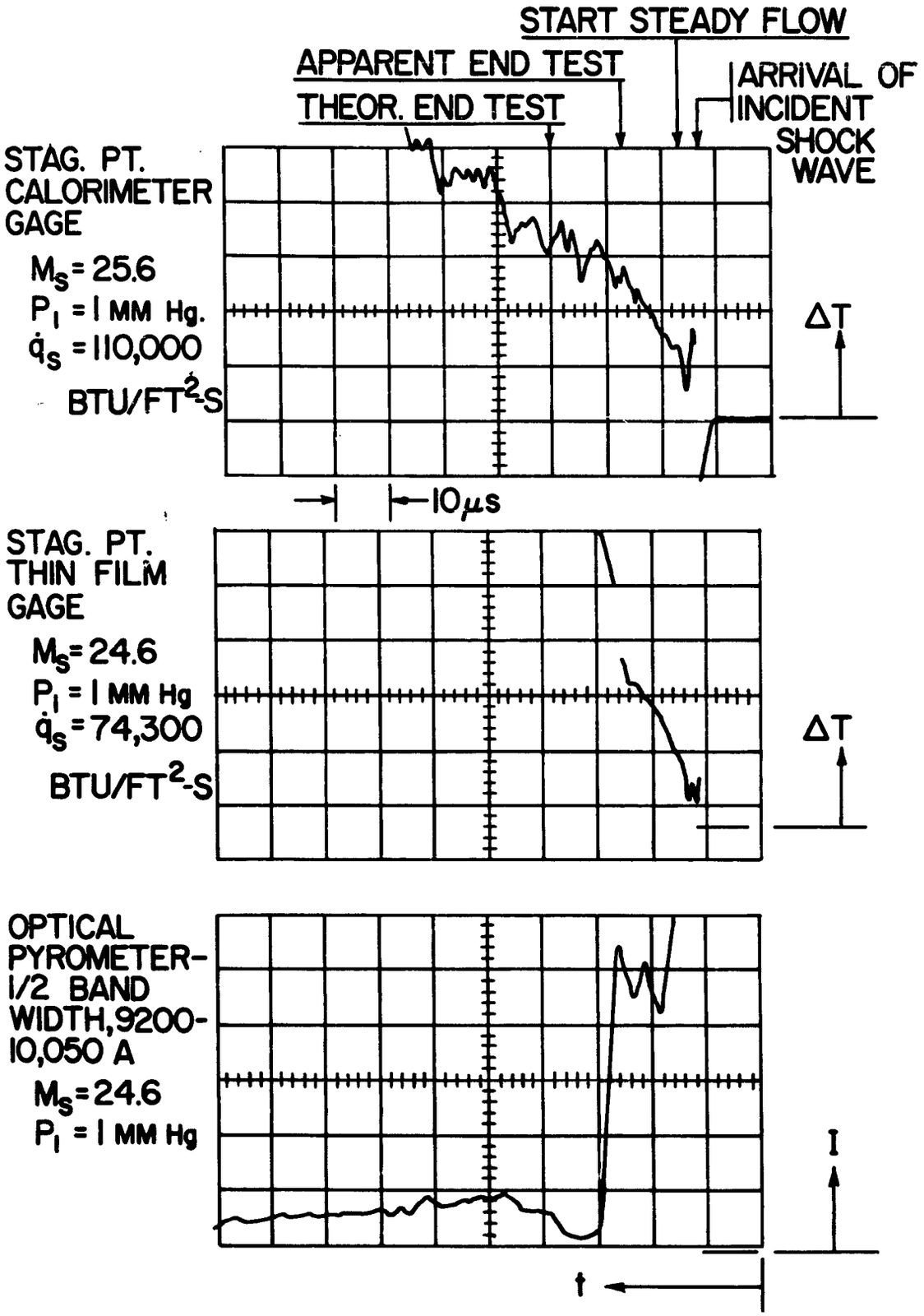

FIGURE 15 MODEL STAGNATION REGION SENSOR SIGNALS

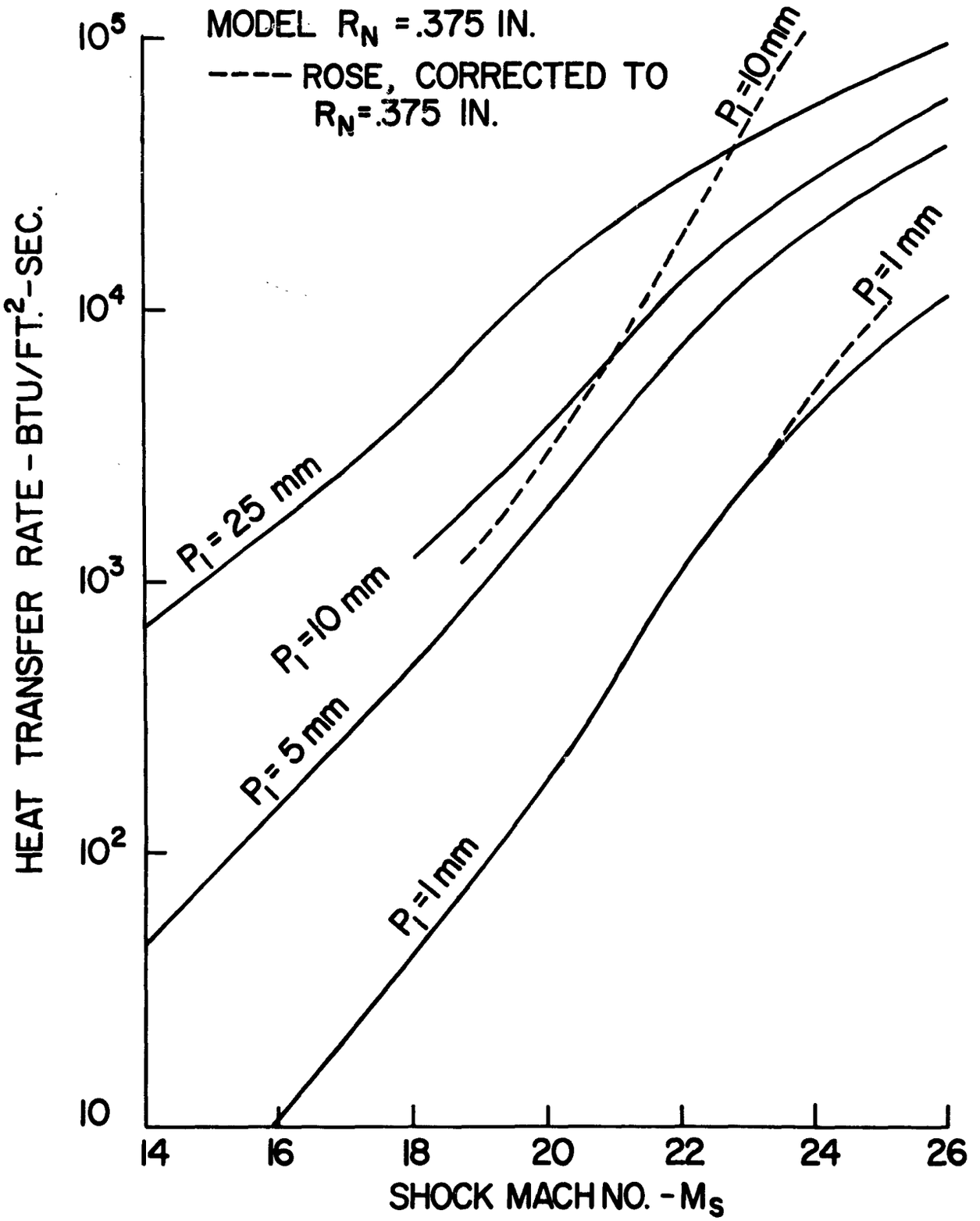

FIGURE 16 EQUILIBRIUM RADIATIVE HEAT TRANSFER AT THE STAGNATION POINT OF THE MODEL

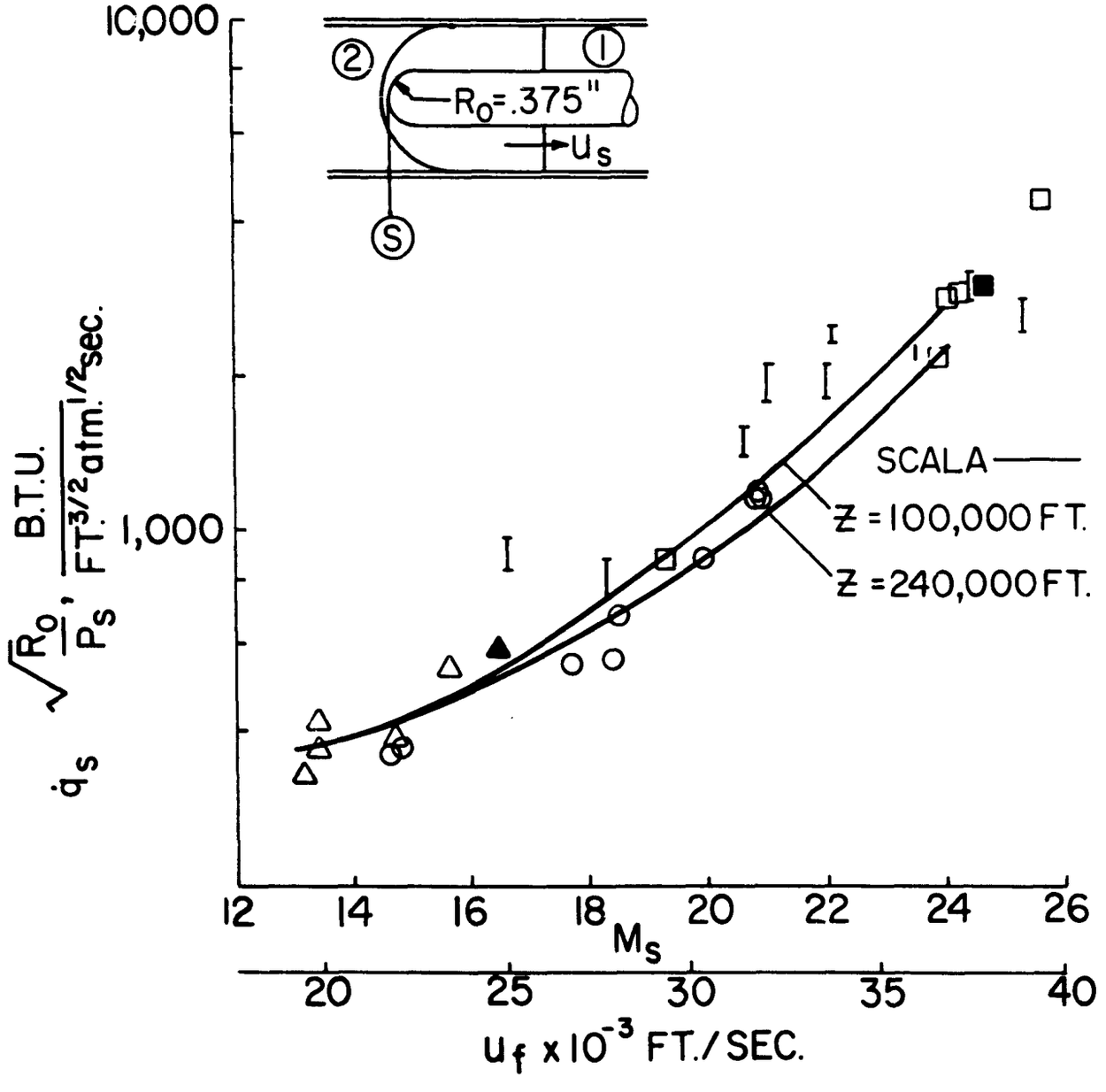

FIGURE 17 STAGNATION POINT HEAT TRANSFER DATA-AIR

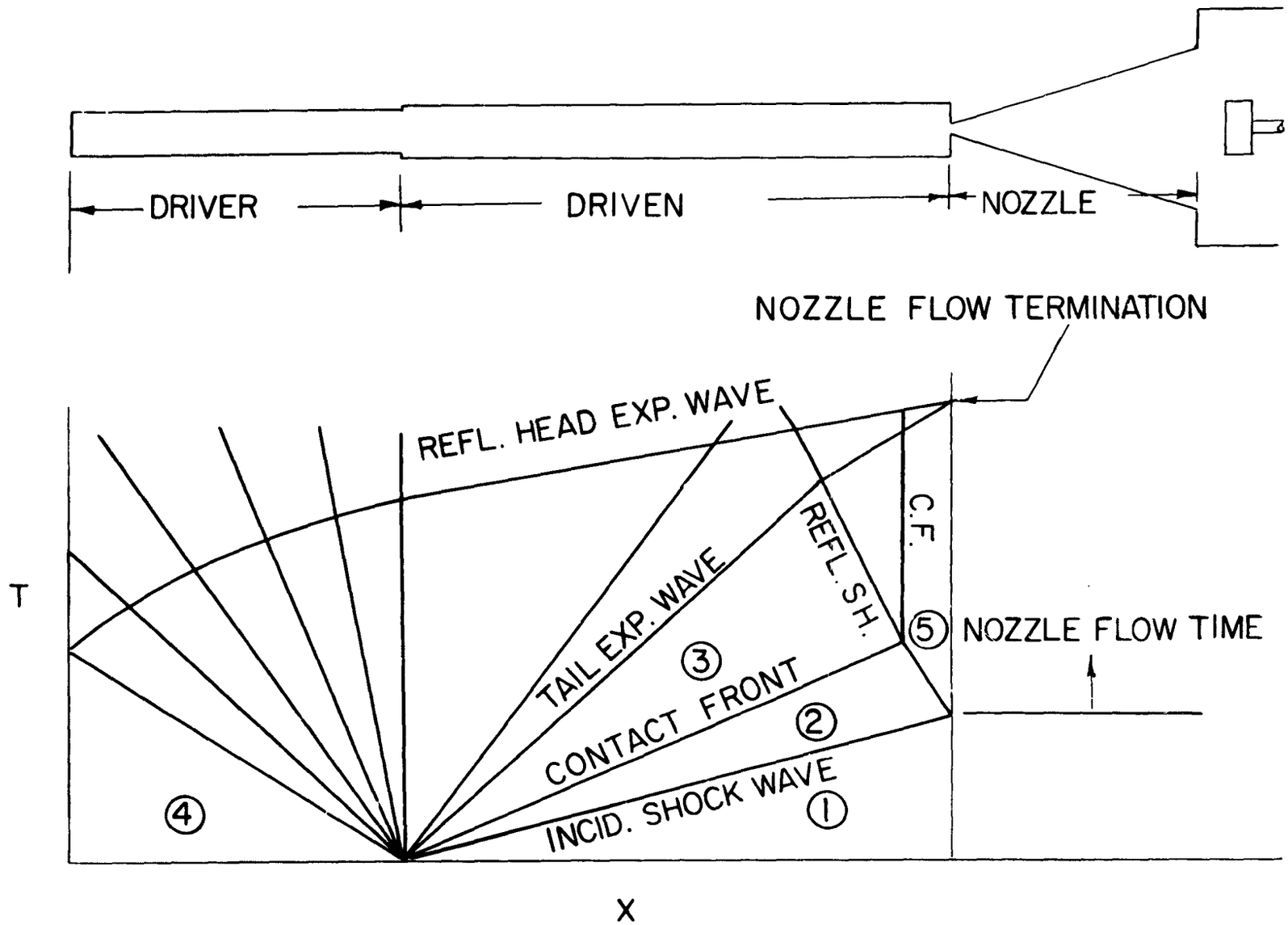

FIGURE 18 REFLECTED SHOCK TUNNEL OPERATION
TAILORED INTERFACE

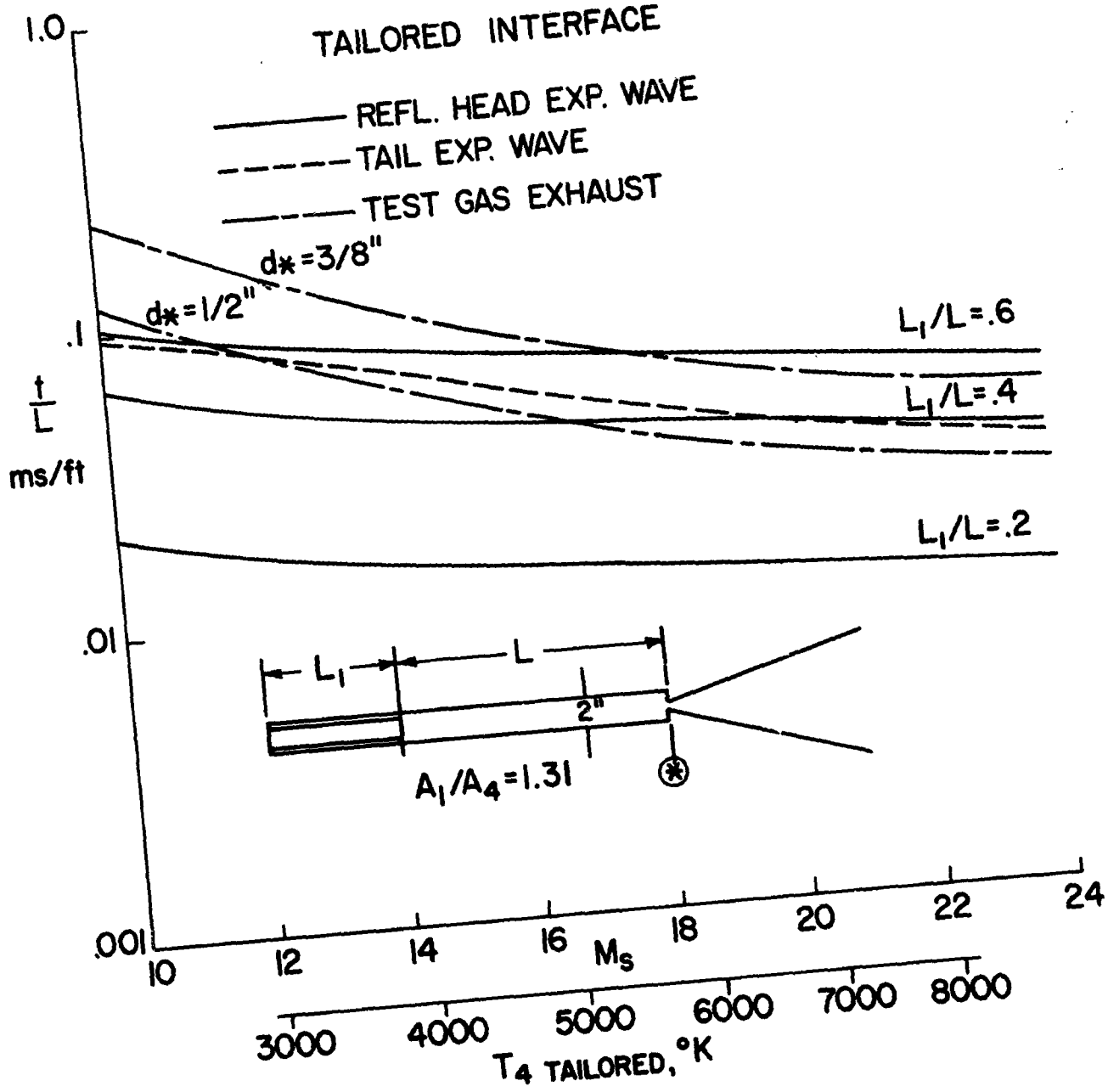

FIGURE 19 NOZZLE FLOW LIMITS - REFLECTED SHOCK TUNNEL

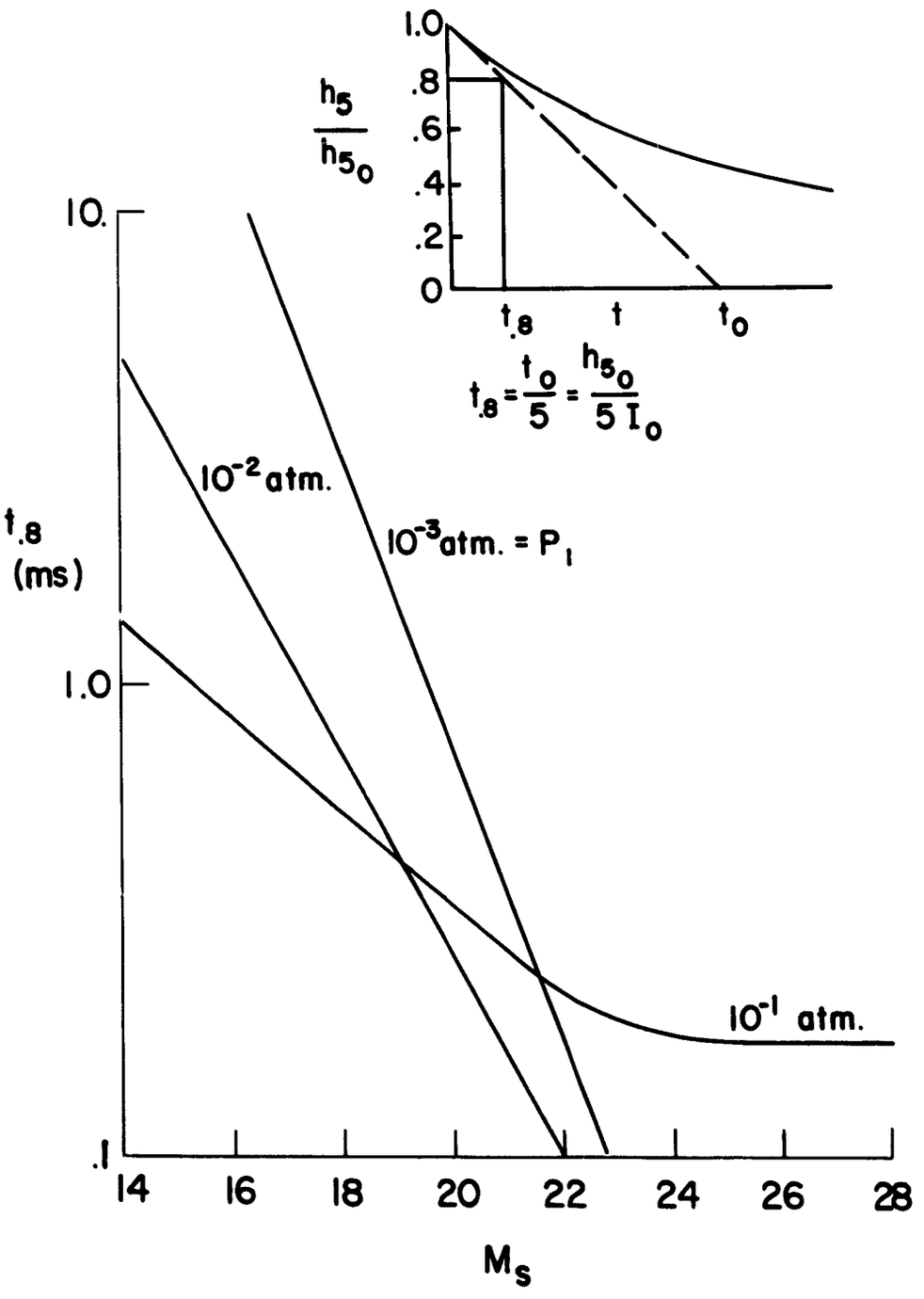

FIGURE 20 ARC HEATED HELIUM DRIVER SHOCK TUBE

HELIUM–AIR SHOCK TUBE

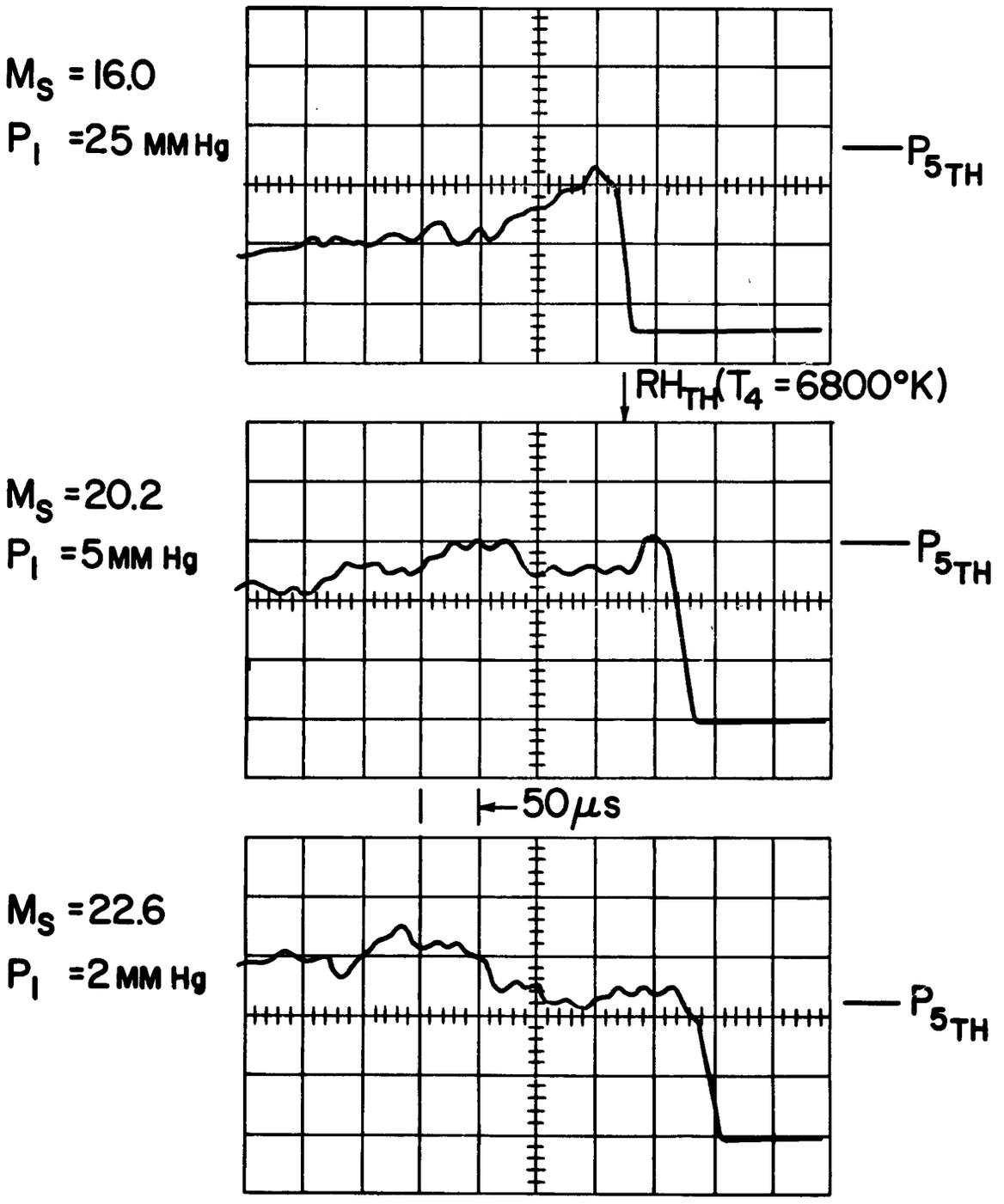

FIGURE 21 PRESSURE RECORDS BEHIND REFLECTED SHOCK WAVE